Energy Reports 7 (2021) 5647–5666

Contents lists available at ScienceDirect

Energy Reports

journal homepage: www.elsevier.com/locate/egyr

Research paper

A reliable and cost-effective planning framework of rural area hybrid system considering intelligent weather forecasting

Ahmadreza Abazari [a], Mohammad Mahdi Soleymani [b], Innocent Kamwa [c,*], Masoud Babaei [b], Mohsen Ghafouri [a], S.M. Muyeen [d], Aoife M. Foley [e,f]

[a] Concordia Institute for Information Systems Engineering (CIISE), Concordia University, Montreal, Canada[1]
[b] Department of Electrical Engineering, Tarbiat Modares University, Tehran, Iran
[c] Department of Electrical Engineering and Computer Engineering, Laval University, Canada
[d] Department of Electrical Engineering, Qatar University, Doha, 2713, Qatar
[e] School of Mechanical and Aerospace Engineering, Queen's University, Belfast, Northern Ireland, BT9 5AH, United Kingdom
[f] Civil, Structural, and Environmental Engineering, Trinity College Dublin, The University of Dublin, Ireland

ARTICLE INFO

Article history:
Received 29 April 2021
Received in revised form 27 August 2021
Accepted 30 August 2021
Available online 10 September 2021

Keywords:
Annualized cost of system
Weather forecasting
Renewable energy penetration
Sensitivity analysis
Meta-heuristic algorithms

ABSTRACT

The use of hybrid systems for electrification of remote areas has been increased dramatically in recent years, and the optimal sizing of these systems is a significant challenge for cost-effectiveness and reliability. This paper aims to propose a predictable planning framework that increases the renewable energy penetration (REP) rate and minimizes the annualized cost of the system (ACS) considering CO_2 emission and different loss of power supply probability (LPSP). Due to the unavailability of precise weather data in remote areas, an intelligent weather forecasting scheme is developed using an adaptive neuro-fuzzy process based on fuzzy c-means clustering technique to estimate the solar radiation, wind speed, and ambient temperature. This paper also examines various evolutionary algorithms and compare the collected result of the proposed Multi-Verse Optimizer (MVO) with other meta-heuristic methods in terms of total annualized cost with different LPSP, and REP amounts. Moreover, to assess the impact of wind speed, solar irradiation, the lifespan of battery energy storage systems, and the fuel price of diesel engine generators on optimal sizing problem, a sensitivity analysis is performed for different values of REP and LPSP. The effectiveness of the proposed approach is verified using a realistic case study in the Sistan & Balouchestan province of Iran. Simulation results illustrate that using photovoltaic panels, wind turbine generators, battery energy storage systems, and diesel engine generators (PV/WTG/BESS/DEG) is the most cost-effective strategy resulting in a 96.13% decrease of CO_2 emission compared to DEG system at $REP_{min} = 97\%$ and $LPSP_{max} = 1\%$. Moreover, the growth of fuel cost causes an increase in the production of renewable energy resources (RESs) and a decrease in the usage of diesel engine generators. Consequently, for $LPSP_{max} = 10\%$ and $REP_{min} = 91\%$, and 50% rise in the price of fuel, the number of DEG drops to zero, and the optimal number of PV and BESS increase from 311 and 172 to 411 and 228, respectively.

1. Introduction

In remote areas, electricity users face various challenges associated with security of energy delivery, and high operational and transmission costs due to economic and geographic reasons (Salameh et al., 2020; Alturki et al., 2021). In this regard, economic planning and optimal sizing of hybrid power systems have been recently proposed as an effective approach to achieve cost-efficient and reliable energy delivery systems in remote areas (Razmjoo et al., 2019; Jamshidi and Askarzadeh, 2019). The optimum size of a hybrid system is a deterministic decision that can be obtained using available energy sources while considering several operational constraints, such as satisfying load demand and reducing costs (Khan et al., 2019). These available energy sources, e.g., diesel engine generators (DEG), battery energy storage systems (BESS), photovoltaic (PV) panels, and wind turbine generators (WTG), are often integrated into the hybrid systems for improving both the reliability and resiliency (Bayani et al., 2021a,b). However, the dependency of wind speed and solar irradiation impose conservative constraints in the calculation of optimal solutions in a power system with the high renewable energy penetration (REP) rate. In this paper, different types of distributed energy resources (DERs), namely, PV, WTG, BESS, and

* Corresponding author.
E-mail address: innocent.kamwa.1@ulaval.ca (I. Kamwa).
[1] https://www.concordia.ca/ginacody/info-systems-eng.html

https://doi.org/10.1016/j.egyr.2021.08.196

Nomenclature

P_{WTG}^{rat}	The rated power of wind turbine generator
P_{WTG}	The output power of wind turbine generator
N_{WTG}	Number of wind turbine generators
E_{WTG}	The total generated power of wind turbine generators
ρ	The density of air
C_p	Power coefficient of wind turbine generator
v	Wind speed at hub height
v_{cut-in}	The cut-in of wind speed
v_r	The rated wind speed
$v_{cut-out}$	The cut-out of wind speed
H	Height of tower where wind turbine generator has been installed
N_{WTG}^{min}	Minimum number of wind turbine generators
N_{WTG}^{max}	Maximum number of wind turbine generators
P_{PV}^{rat}	The rated power of photovoltaic panel
P_{PV}	The output power of photovoltaic panel
N_{PV}	Number of photovoltaic panels
E_{PV}	The total generated power of photovoltaic panels
$NOCT$	Normal operating cell temperature of photovoltaic panel
I^{ref}	Solar radiation at reference condition
T_{ref}	Standard temperature
I	Solar irradiation
T_{cell}	The temperature of cell
α	The temperature coefficient of photovoltaic panels
T	Ambient temperature
N_{PV}^{min}	Minimum number of photovoltaic panels
N_{PV}^{max}	Maximum number of photovoltaic panels
E_{Batt}	Level of charge of battery
σ	The rate of self-discharge of battery
η_{Batt}	The efficiency of charge state of battery
N_{Batt}	Number of battery energy storage systems
N_{Batt}^{min}	Minimum number of battery energy storage systems
N_{Batt}^{max}	Maximum number of battery energy storage systems
E_{Batt}^{min}	The minimum level of charge of battery energy storage system
E_{Batt}^{max}	The maximum level of charge of battery energy storage system
S_{Batt}^{rat}	The nominal capacity of battery energy storage system
DOD	Maximum depth of discharge of battery energy storage system
$Cons_{DEG}$	The fuel consumption of diesel engine generator
A_D, B_D	Coefficients of the consumption curve
P_{DEG}^{rat}	The nominal output power of diesel engine generator
P_{DEG}	The power of diesel engine generator
N_{DEG}	Number of diesel engine generators
N_{DEG}^{min}	Minimum number of diesel engine generators
N_{DEG}^{max}	Maximum number of diesel engine generators
η_{Inv}	Efficiency of inverter
E_{Load}	Load demand
E_{ren}	The total generated power of renewable energy sources
CC_k	Capital cost related to each unit
ACC_k	Annual capital cost related to each unit
CRF	Capital recovery factor
ir	Annual real interest rate
t_l	Lifetime of project
i	Nominal interest rate
f	Annual inflation rate
$RC_{k_{rep}}$	Replacement cost related to each unit that needs to be replaced
$ARC_{k_{rep}}$	Annual replacement cost related to each unit that needs to be replaced
SFF	Sinking fund factor
t_{rep}	The lifespan of each unit that needs to be replaced
P_{fuel}	Cost of fuel per liter
FC	Cost of fuel consumption of diesel engine generators
AFC	Annual fuel cost related to diesel engine generators
$AO\&MC$	Annual operation & maintenance cost related to each unit
$LPSP_{max}$	Maximum loss of power supply reliability
REP_{min}	Minimum renewable energy penetration
$NI\ (U_i)$	The normalized inflation rate of U matrix
r_1, r_2, r_3, r_4	Random numbers in the range of 0 and 1
X_j	The jth parameter of the best universe
x_i^j	The jth parameter of ith universe
lb_j	The lower bound of jth variable
ub_j	The upper bound of jth variable
WEP_{min}	Minimum value of wormhole existence probability factor
WEP_{max}	Maximum value of wormhole existence probability factor
l	The current number of iterations
L	The maximum number of iterations
p	The exploitation accuracy
m	The number of vector data of FCM
c	The number of cluster of FCM
μ_{ij}	Membership degree of data point j in cluster i
q	The index of fuzziness fluctuating in the range $[1, \infty]$

d_{ij}	Euclidean distance between c_i and x_j
$O_{i,1}$	The first layer output of ANFIS
X, Y	Incoming signals
$\overline{w}_i$	Normalized firing strength

Subscript

n	The number of universes
d	The number of optimization parameters of MVO

Abbreviation

WTG	Wind Turbine Generator
PV	Photovoltaic
BESS	Battery Energy Storage System
DEG	Diesel Engine Generator
FC	Fuel Cell
DER	Distributed Energy Resource
DG	Distributed Generation
RES	Renewable Energy Source
NPC	Net Present Cost
TNPC	Total Net Present Cost
TAC	Total Annual Cost
EENS	Expected Energy Not Supplied
ELF	Equivalent Loss Factor
LOLE	Loss Of Load Expected
LCE	Levelized Cost of Energy
REP	Renewable Energy Penetration
LPS	Loss of Power Supply
LPSP	Loss of Power Supply Probability
MVO	Multi-Verse Optimizer
DA	Dragonfly Algorithm
GOA	Grasshopper Optimization Algorithm
GWO	Grey Wolf Optimization
SSA	Salp Swarm Algorithm
GA	Genetic Algorithm
PSO	Particle Swarm Optimization
HS	Harmony Search
MILP	Mixed Integer Linear Programming
EHO	Elephant Herding Optimization
CSA	Crow Search Algorithm
CS	Cuckoo Search
WEP	Wormhole Existence Probability
TDR	Traveling Distance Rate
ANN	Artificial Neural Network
FIS	Fuzzy Inference System
RBF	Radial Basis Function
ANFIS	Adaptive Neuro-Fuzzy Inference System
FCM	Fuzzy C-Means
ANFIS-FCM	Adaptive Neuro-Fuzzy Inference System based on Fuzzy C-Means
MF	Membership Function
MSE	Mean Square Error
RMSE	Root Mean Square Error
STD	Standard Deviation

DEG as a backup generation unit are deployed. From this perspective, resolving a multifaceted planning framework, which can increase the REP rate by minimization of the annualized cost of the system (ACS) is a vital issue. It is worth mentioning that ACS also considers carbon emission and different loss of power supply probability (LPSP).

Several hybrid energy systems, which have been studied in recent papers, utilize DERs, e.g., wind, solar, hydrogen, battery, and diesel generator, to resolve several challenges of electricity demand effectively (Babaei et al., 2021; Alberizzi et al., 2020). The problem of the economic sizing of a hybrid power system with a non-convex nature has been addressed through effective methods in the literature (Foley et al., 2010). The existing methods consider a wide range of modern hybrid systems including hybrid optimization model for electric renewables (HOMER) (Das and Zaman, 2019; Haratian et al., 2018), linear and non-linear programming (Roy, 1997; Mohammadi et al., 2017), mixed integer linear programming (MILP) (Alberizzi et al., 2020), genetic algorithm (GA) (Suresh et al., 2020), particle swarm optimization (PSO) (Askarzadeh and dos Santos Coelho, 2015), elephant herding optimization (EHO) (Ashraf et al., 2020), crow search algorithm (CSA) (Ghaffari and Askarzadeh, 2020), cuckoo search (CS) (Sanajaoba Singh and Fernandez, 2018), and harmony search (HS) (Maleki and Askarzadeh, 2014b). Furthermore, meta-heuristic algorithms have received a high surge of attention due to unparalleled capabilities at different levels of hybrid power systems (Bala and Siddique, 2009; Maleki and Askarzadeh, 2014a). For instance, in Hossain et al. (2019), authors have developed slow-paced algorithms to facilitate the analysis of cost function and reduce the electricity cost of a microgrid by about 12% compared to other proposed methods; however, Multi-Verse Optimizer (MVO) in many works , such as extracting several parameters of PV arrays and task scheduling in cloud computing environments, yields a promising performance in terms of convergence speed, minimization of execution time, cost, and best solutions compared to other mentioned optimization algorithms (Ali et al., 2016; Shukri et al., 2021). Recently, different participation indexes, which can increase the reliability of power systems considerably, have been also reported. As an example, authors in Sanajaoba and Fernandez (2016) have considered total system cost as an objective function and defined two standards including loss of load expected (LOLE) and expected energy net supplied (EENS) as reliability. In Askarzadeh (2017), the crow search algorithm is applied in PV/WTG/BESS/Tidal hybrid system to minimize the net present cost (NPC) by considering equivalent loss factor (ELF). Besides, LPSP is a commonly used reliable factor in a wide range of recent investigations (Ghorbani et al., 2018; Maleki and Pourfayaz, 2015). It is worth mentioning that different criteria and optimization algorithms can be proposed to improve the reliability of a hybrid system based on the type of geographical location and facilities.

Environmental emission is another significant factor that has recently received a high level of attention in the analysis of hybrid systems. In Hafez and Bhattacharya (2012), optimal sizing is modeled based on the lifecycle costs and environmental constraints using HOMER Pro software. In Movahediyan and Askarzadeh (2018), objective functions of optimal planning are defined according to three different criteria, i.e., carbon emission, total net present cost, and LPSP in a hybrid system. Moreover, to make a confident prediction of the future performance of hybrid systems during various operational conditions, sensitivity analysis of parameters can be introduced as a practical approach in several studies. This sensitivity analysis method is implemented for several operating conditions, i.e. wind speed, solar irradiation, CO_2 emission, the price of fuel, the capital cost of the system component, and load consumption. However, sensitivity analysis has not been represented in the presence of different values of REP and LPSP in a hybrid system. In addition, the effect of battery lifespan on optimal sizing problem has not been broadly studied in previous studies. As a result, in this project, we try to address these concerns in a remote area efficiently.

Despite many papers have focused on the capabilities of RESs to improve the performance of recent hybrid systems, there is a lack of cost-effective and reliable models suitable for distant areas (Zhang et al., 2018). In this regard, a cost-effective hybrid model can be firstly introduced in our project, and then available resources are selected based on optimization approaches to study both technical and economic aspects of this distant hybrid system. In Zhang et al. (2019), authors have deployed a new renewable energy source, i.e., hydrogen energy systems, which can result in a considerable increase in the total cost of hybrid systems. Using such a DER makes the hybrid system costly for remote areas of a country. Another group of researchers have neglected the long-term optimal planning and focused on the optimum combination of RESs in hybrid power systems for a short time span (Ranjbar et al., 2014; Ranjbar and Kouhi, 2015; Stoppato et al., 2014). In fact, a significant number of works have investigated a small snapshot of an operating moment of hybrid systems which may not proper for a local area. Furthermore, several studies have ignored the impact of weather forecasting and climatic changes in their optimal sizing (Kazem et al., 2013). Since the weather data for renewable energies in remote areas are not accessible with ease, intelligent weather forecasting methods must be introduced to improve the precision of our optimal sizing of hybrid systems. One of a modified type of an adaptive neuro-fuzzy inference system (ANFIS), which is widely used in prediction mechanisms, is an ANFIS-FCM (fuzzy c-means) approach. This method has been received a special consideration in several prediction procedures such as anticipation of earthquake magnitude and thermal error in industrial automation (Mirrashid, 2014; Abdulshahed et al., 2015a). In fact, the fuzzy c-means (FCM) technique could decrease the number of rules and network complexity, and consequently increase the speed of prediction mechanisms.

In this manuscript, we suggest a wide range of distributed energy resources (DERs) to constitute a hybrid system owing to windy areas and deserts in the under-study province. Additionally, MVO algorithm is deployed to improve the optimization process of our hybrid system planning. Inspiring from the above discussion, the intermittent nature of wind speed and solar irradiation could add various uncertainties to our hybrid system. As a result, the mentioned data must be efficiently predicted using ANFIS-FCM. In this regard, the main contribution of this paper with considering above-mentioned concerns, i.e., the speed of optimization process of planning framework and lack of weather data in remote areas, can be listed as follows:

- Addressing previous deficiencies in the modeling of renewable energies by considering the potential of distributed generations and designing a specific optimal sizing for this area.
- Proposing an adaptive neuro-fuzzy method according to fuzzy c-means (ANFIS-FCM) clustering technique to tackle the problem of data unavailability for solar radiation, wind speed, and ambient temperature in remote areas.
- Proposing an optimal scheme of an off-grid hybrid system to study the desired values of LPSP and REP, CO_2 emission, and total system cost based on different RESs combinations. To resolve this economic-environmental-energy sizing problem, one of the efficient meta-heuristic algorithms, i.e., Multi-verse optimizer (MOV) is introduced in a realistic case study in the Sistan & Balouchestan province of Iran.
- Conducting a sensitivity analysis for variation of wind speed, solar radiation, the lifespan of battery energy storage systems, and the cost of fuel to assess the optimal sizing problem in case of different values of REP and LPSP.

2. Hybrid system configuration

A case study that represents a distant area in Sistan & Balouchestan province is adopted so as to investigate the performance of the proposed technique. The layout of this system including its several energy sources, e.g. wind turbine generator, solar parks, battery, and diesel engine generator is illustrated in Fig. 1. In this scheme, wind turbine generators and solar panels are responsible for producing clean energy and meeting the load demand. Battery energy storage systems can store extra electricity energy and guarantee the reliability and stability of the hybrid system in a fairway, and diesel engine generator can play a supportive role during various operational conditions in this hybrid system. Moreover, a high percentage of controllable and non-controllable appliances deploy AC power, consequently, inverter-based topologies are introduced to meet this need practically.

2.1. Modeling of wind turbine generator

Recently, WTG has witnessed significant growth for two important reasons; (i) WTG can reduce the volume of air pollution and remove environmental concerns to a great extent, and (ii) WTGs are generally considered as efficient economic sources of energy. Wind speed could change greatly due to its fluctuating nature at different times of the day. In this regard, the output power related to wind turbine generators is proposed as a variable energy source in integrated hybrid systems. From this perspective, WTG starts to produce electrical energy when wind speed exceeds the cut-in value. In the following, WTG generates a constant value, when wind speed exceeds the rated speed and if the speed of wind reaches the cut-out value, it will stop smoothly to prevent any damage to the mechanical structure (Lee and Wang, 2008). This nominal output power can be expressed as follows (Abazari et al., 2020):

$$P_{WTG}^{rat} = \frac{1}{2} \times \rho \times A \times C_p \times v^3 \tag{1}$$

where in Eq. (1), ρ, A, C_p, and v are the density of air (kg/m^3), the swept area of wind turbine (m^2), WTG power coefficient, and nominal wind speed (m/s), respectively.

The power generated of WTG during various operational conditions, can be calculated at any wind speed by the following equation (Maleki and Pourfayaz, 2015; Arzani et al., 2021):

$$P_{WTG}(t) = \begin{cases} 0 & v(t) < v_{cut-in} \\ av(t)^3 - bP_{WTG}^{rat} & v_{cut-in} < v(t) < v_r \\ P_{WTG}^{rat} & v_r \le v(t) \le v_{cut-out} \\ 0 & v(t) > v_{cut-out} \end{cases} \tag{2}$$

where two parameters (a, b) in (2) can be defined as:

$$a = {}^{P_{WTG}^{rat}}/\left(v_r^3 - v_{cut-in}^3\right) \tag{3}$$

$$b = {}^{v_{cut-in}^3}/\left(v_r^3 - v_{cut-in}^3\right) \tag{4}$$

$$v(t) = v_0(t) \times ({}^{H}/_{H_0})^{\alpha} \tag{5}$$

In Eqs. (2) to (5), v is the wind speed at hub height (m/s), H is the height of the tower (m) where this WTG has been installed, α is the wind shear coefficient which is assumed to be 0.25 in this paper and P_{WTG}^{rat} is defined as the rated power of the wind turbine generator ($watt$) based on Eq. (1). In addition, v_r, v_{cut-in}, and $v_{cut-out}$ represent the rated, cut-in, and cut-out of wind speed (m/s), respectively.

In this hybrid system, assuming N_{WTG} to be the number of wind turbine generators, the total generated power can be expressed as:

$$E_{WTG}(t) = N_{WTG} \times P_{WTG}(t) \tag{6}$$

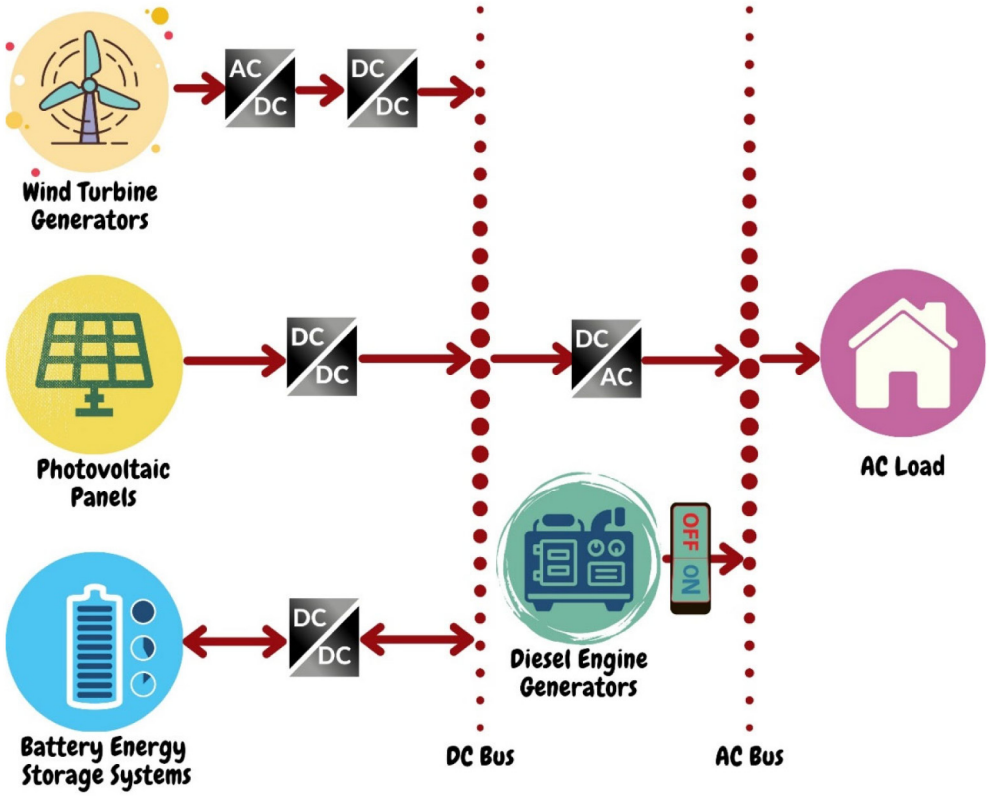

Fig. 1. The layout of a hybrid power system in a remote area of Sistan & Balouchestan province.

2.2. Modeling of photovoltaic panels

Solar radiation must be considered in a pragmatic way to present a proper PV model in a hybrid system. As a result, the output active power related to solar cells can be obtained by the following equation (Maleki and Pourfayaz, 2015):

$$P_{PV}(t) = P_{PV}^{rat} \times ({}^{I(t)}/_{I^{ref}}) \times \left[1 + \alpha\left(T_{cell}(t) - T_{ref}\right)\right] \tag{7}$$

where solar irradiation is indicated as $(I(t))$ in (W/m^2) and I^{ref} is the solar radiation at reference condition (1000 W/m^2). T_{ref} is defined as the standard temperature (°C) and α is the PV temperature coefficient. In addition, the temperature of cell (T_{cell}) can be introduced as (Maleki and Pourfayaz, 2015):

$$T_{cell}(t) = T(t) + ({}^{I(t)}/_{800}) \times (NOCT - 20) \tag{8}$$

It is important to mention that $NOCT$ is proposed as the normal operating cell temperature in °C and $T(t)$ is defined as a function which states ambient temperature.

If the number of solar panels is N_{PV}, the total power which is generated through solar energy can be given by:

$$E_{PV}(t) = N_{PV} \times P_{PV}(t) \tag{9}$$

2.3. Modeling of battery energy storage system

One of the advantages of using a low-inertia hybrid system is to consider the effect of energy storage systems, i.e. BESSs, along with DERs. The storage systems can be deployed with non-dispatchable DER units like wind farms and solar parks to turn them into dispatchable ones. Under this circumstance, the battery starts to store electrical energy, if the total power is greater than demand on the load side. On the contrary, if the total of generated energy is less than demand, the battery will enter the discharge state to keep a balance between demand and consumption rate. For the aforementioned states, the charge and discharge level of this battery energy storage in a hybrid system can be expressed by the following equations (Maleki and Askarzadeh, 2014b):

For charge state:

$$E_{Batt}(t) = E_{Batt}(t-1) \times (1-\sigma) + \Big((E_{PV}(t) \times \eta_{Inv} + E_{WTG}(t) \times \eta_{Inv}^2) - {}^{E_{Load}(t)}/_{\eta_{Inv}} \Big) \times \eta_{Batt} \tag{10}$$

For discharge state:

$$E_{Batt}(t) = E_{Batt}(t-1) \times (1-\sigma) - \left({}^{E_{Load}(t)}/_{\eta_{Inv}} - \left(E_{PV}(t) \times \eta_{Inv} + E_{WTG}(t) \times \eta_{Inv}^2\right)\right) / \eta_{Inv} \tag{11}$$

In the above-mentioned equations, $E_{Batt}(t)$ and $E_{Batt}(t-1)$ represent the level of charge of the battery at t and $t-1$, respectively. The rate of self-discharge can be defined as σ and presented based on the hour unit. Furthermore, η_{Inv} and η_{Batt} indicate the efficiency of the inverter and charge state of the battery, respectively. In Eq. (11), the discharge efficiency of the battery energy storage system is assumed as unity. Finally, $E_{Load}(t)$ in both equations is a symbol of load demand.

2.4. Modeling of diesel engine generator

In this hybrid system, the diesel engine generator is proposed as a fast power injection component to prevent any deficiency or blackout on the load side. This type of energy generation starts to produce electricity, when WTG and PV cannot participate in the energy production scheme and the state of the battery energy storage system is low. The fuel consumption of DEG (Liter), which depends on output power and several coefficients of the consumption curve (A_D *and* B_D), mentioned in references (Jamshidi and Askarzadeh, 2019; Ashraf et al., 2020):

$$Cons_{DEG}(t) = A_D \times P_{DEG}^{rat} + B_D \times P_{DEG}(t) \tag{12}$$

In this equation, P_{DEG}^{rat} is the nominal DEG output power and $P_{DEG}(t)$ is defined as a power of DEG at time t.

3. Optimization problem formulation

3.1. Cost modeling

In this manuscript, the minimization of annualized cost of the system is considered as the main objective function. The total cost consists of annual capital cost (ACC), annual operation and maintenance cost ($AO\&MC$), annual replacement cost (ARC) as well as annual fuel consumption cost (AFC) related to diesel engine generator. For this hybrid system, which comprises different renewable energy sources, the annualized cost of this hybrid system can be calculated as:

$$ACS = ACC + AO\ MC + ARC + AFC \tag{13}$$

In this analysis, replacement costs are only considered for the battery, DEG, and inverter. The main reason is that the lifespan of the wind turbine generators, as well as photovoltaic panels, is relatively long and equal to the lifetime of this project in the Sistan & Balouchestan province. From this perspective, the longevity of battery, inverter, and DEG is 5 years, 10 years, and 15,000 h, respectively.

3.1.1. Capital cost

The amount of annual capital cost related to each unit (WTG, PV, BESS, DEG, and inverter) in this system considering the installation costs in the site can be calculated as below (Ashraf et al., 2020):

$$ACC_k = CC_k \times CRF(ir, t_l) \tag{14}$$

where CC_k is the capital cost in relation to each unit and $CRF(ir, t_l)$ is defined as a capital recovery factor to change the initial capital cost into the annual capital cost as well. This factor generally is associated with the annual real interest rate (ir) and longevity of the project (t_l):

$$CRF(ir, t_l) = {}^{(ir\times(1+ir)^{t_l})}/_{((1+ir)^{t_l}-1)} \tag{15}$$

It should be noted that the annual interest rate is associate with a nominal interest rate (i) and annual inflation rate (f) as:

$$ir = {}^{(i-f)}/_{(1+f)} \tag{16}$$

3.1.2. Replacement cost

In this case study, several units including battery, diesel engine generator, and inverter may be replaced with new energy production units. As a result, the annual replacement cost of such gadgets can be obtained by the following equation (Ashraf et al., 2020):

$$ARC_{k_{rep}} = RC_{k_{rep}} \times SFF(ir, t_{rep}) \tag{17}$$

where $RC_{k_{rep}}$ is the replacement cost of mentioned units and $SFF(ir, t_{rep})$ is defined as sinking fund factor which is associated with the annual real interest rate (ir) and longevity of each assumed units (t_{rep}) (Ashraf et al., 2020).

$$SFF\left(ir, t_{rep}\right) = {}^{ir}/_{((1+ir)^{trep}-1)} \tag{18}$$

3.1.3. Cost of fuel consumption

The hourly cost of fuel consumption can be presented by the following statement (Maleki and Askarzadeh, 2014b):

$$FC\ (t) = P_{fuel} \times Cons_{DEG}(t) \tag{19}$$

In this manuscript, P_{fuel} is referred to as the cost of fuel per liter. Consequently, the annual fuel cost for this diesel engine generator is calculated as:

$$AFC = \sum_{t=1}^{8760} FC(t) \tag{20}$$

3.2. Objective function

In this case study, the main aim is to optimize the number of renewable energy sources and diesel engine generators in a hybrid system to minimize the annualized cost. As a result, the objective function related to this case study can be defined as:

$$Min[ACS\ (N_{PV}, N_{WTG}, N_{Batt}, N_{DEG})] = Minimize\left[\left(\sum_{k=PV,WTG,Batt,DEG,Inv} N_k \times (ACC_k + AO\ MC_k)\right) + \left(\sum_{k_{rep}=Batt,DEG,Inv} N_{k_{rep}} \times ARC_{k_{rep}}\right) + AFC\right] \tag{21}$$

Several constraints should be satisfied for WTG, PV, BESS as well as diesel engine generator system in order to optimize this objective function effectively:

$$N_{WTG} = Integer \qquad N_{WTG}^{min} \le N_{WTG} \le N_{WTG}^{max} \tag{22}$$

$$N_{PV} = Integer \qquad N_{PV}^{min} \le N_{PV} \le N_{PV}^{max} \tag{23}$$

$$N_{Batt} = Integer \qquad N_{Batt}^{min} \le N_{Batt} \le N_{Batt}^{max} \tag{24}$$

$$N_{DEG} = Integer \qquad N_{DEG}^{min} \le N_{DEG} \le N_{DEG}^{max} \tag{25}$$

At different times, the level of the charge state of BESS must be satisfied as below:

$$E_{Batt}^{min} \le E_{Batt}\ (t) \le E_{Batt}^{max} \qquad t\epsilon[1, 8760] \tag{26}$$

where E_{Batt}^{min} and E_{Batt}^{max} indicate the minimum and maximum level of charge of BESS, respectively. The maximum level of charge is defined based on the nominal capacity of BESS (S_{Batt}^{rat}) and the minimum level can be acquired by the maximum depth of discharge (DOD) in order to extend the longevity of BESS and protect against unwanted events (Khan et al., 2019):

$$E_{Batt}^{min} = (1 - DOD) \times S_{Batt}^{rat} \tag{27}$$

3.2.1. Reliability, environmental and renewable energy penetration constraints

The LPSP, as a metric, can be leveraged to evaluate the reliability of the system practically. This criterion is a number that varies between 0 and 1. The LPSP of 0 means that the demand will be satisfied completely and the LPSP of 1 states the condition in which no portion of demand is satisfied. As a consequence, LPSP can be presented based on a specific time interval (Jamshidi and Askarzadeh, 2019):

$$LPSP = {}^{\sum_{t=1}^{T} LPS(t)}/_{\sum_{t=1}^{T} E_{Load}(t)} \tag{28}$$

Another concept, i.e., loss of power supply ($LPS(t)$), is introduced when the total generated energy and the amount of energy saved in the battery is less than the amount of load demand:

$$LPS\ (t) = {}^{(E_{Load}(t)-E_{DEG}(t))}/_{\eta_{Inv}}) - \left(E_{PV}\ (t) \times \eta_{Inv} + E_{WTG}\ (t) \times \eta_{Inv}^2\right) - \left(E_{Batt}\ (t-1) - E_{Batt}^{min}\right) \tag{29}$$

The mass of emitted CO_2 can be calculated as follows (Jamshidi and Askarzadeh, 2019):

$$CO_{2w} = {}^{(CC\times E_{DEG})}/_{1016.04} \tag{30}$$

where CC, E_{DEG}, and CO_{2w} indicate carbon content (0.6078 kg/kWh), the total power which is generated by DEG, and carbon weight (ton), respectively.

Another new concept, which can play an important role in using the full potential of installed RESs and generating clean energy, is renewable energy penetration. A high percentage of organizations are enforced to supply a portion of their consumption using renewable energy sources. Consequently, this parameter is defined to satisfy the pre-defined desired value as discussed in Ghaffari and Askarzadeh (2020):

$$REP = \sum_{t=1}^{T}\left(E_{PV}(t)\times\eta_{Inv}+E_{WTG}(t)\times\eta_{Inv}^{2}\right)/\sum_{t=1}^{T}\left(E_{PV}(t)\times\eta_{Inv}+E_{WTG}(t)\times\eta_{Inv}^{2}+E_{DEG}(t)\right) \tag{31}$$

In a hybrid system, a consumer generally defines the concept of $LPSP_{max}$ during optimization technique. To guarantee the reliability of the system, one constraint should be considered in order to satisfy the maximum loss of power supply reliability:

$$LPSP \leq LPSP_{max} \tag{32}$$

Furthermore, other constraint on CO_2 is defined to satisfy the maximum desired carbon weight as follows:

$$CO_{2w} \leq CO_{2w}^{max} \tag{33}$$

Moreover, another constraint is considered for renewable energy penetration:

$$REP \geq REP_{min} \tag{34}$$

where REP_{min} means minimum the desired share of this type of clean energy.

4. Energy management strategy

The proposed strategy to achieve an acceptable performance can be introduced and categorized in four conditional energies situations as follow:

1. If the calculated generated power by Eq. (35) from renewable energy sources is more than load demand, extra power can be stored in BESS until the level of charge of BESS reaches E_{Batt}^{max}. By BESS reaching to this level of charge, the excess power generation is sent to the dump load. It should be a notion that renewable energy sources are a combination of WTGs and PV panels.
2. In this case, power generation of renewable energy sources is lower than load demand. But the available energy of BESS and generated power from RESs which are calculated by Eq. (36), are sufficient for load demand. Therefore, BESS will enter the discharge state, and BESS's level of charge is updated by Eq. (11).
3. If generated power of RESs and the available energy of BESS is lower than the load demand, diesel engine generators will start to generate electricity in order to meet all the considered requirements. This case is divided into the following two cases:
    - 3.1. If calculated power generation by Eq. (37) from RESs and DEGs meets load demand, the extra generated power is used to charge BESS. The mentioned charging will continue till the state level reaches E_{Batt}^{max}. By reaching this level, the excess power generation is sent to the dump load.
    - 3.2. If generated power of RESs and DEGs are lower than load demand, BESS will enter the discharge state. Consequently, the level of charge of BESS is updated by Eq. (11).
4. If total power generated by PV panels, WTGs, DEGs, and BESS, with regard to the minimum permissible discharge, are not able to supply all load demand, some of the load is not supplied. Therefore, the loss of power supply (LPS) occurs.

Finally, if the fitness function including objective function and constraints is satisfied, optimization will be completed. These scenarios have been summarized and depicted through a flowchart in Fig. 2.

$$E_{re}(t) = \left(E_{PV}(t)\times\eta_{Inv} + E_{WTG}(t)\times\eta_{Inv}^{2}\right)\times\eta_{Inv} \tag{35}$$

$$E_{re+b}(t) = \eta_{Inv}^{2}\times E_{Batt}(t-1)\times(1-\sigma) + E_{ren}(t) - \eta_{Inv}^{2}\times E_{Batt}^{min} \tag{36}$$

$$E_{re+d}(t) = E_{ren}(t) + (N_{DEG}\times P_{DEG}(t)) \tag{37}$$

4.1. Different types of optimization tools

In this practical project, the economic sizing of our hybrid system can be achieved by minimizing the annualized cost of the system, a reliable amount of LPSP, and the maximum possible of REP. To provide superior optimization tools, several advanced meta-heuristic methods, e.g. grasshopper optimization algorithm (GOA) (Saremi et al., 2017), grey wolf optimization (GWO) (Mirjalili et al., 2014), dragonfly algorithm (DA) (Mirjalili, 2016), salp swarm algorithm (SSA) (Mirjalili et al., 2017), are introduced, and their performance is compared to multi-verse optimizer (MVO) for different simulation scenarios.

4.1.1. Multi-Verse optimizer

Multi-Verse theory is derived from the big bang theory, which states that the universe has been created due to a tremendous explosion. This nature-inspired algorithm originates from multi-verse theory in physics, and it is based on three concepts in cosmology, including white hole, black hole, and wormhole. White holes, which are the main factor, are able to create the universe. Black holes can drag everything towards themselves because of gravitational forces and wormholes are able to keep contact with different universes together as well as moving objects towards different universes. The universe can be expanded in space practically due to its constant rate which is referred to as inflation. It is important to mention that for achieving a balance between different universes, all black, white, and wormholes should be in contact with each other. According to the relationship between the inflation rate and holes, the following rules are applied to the universes for the optimization process (Mirjalili et al., 2016):

1. The probability of the existing white hole can increase by raising the inflation rate.
2. The probability of the existing black hole can decrease by raising the inflation rate.
3. In a universe, white holes send objects with high inflation.
4. In a universe, black holes receive objects with a low inflation rate.
5. Without considering the inflation rate, objects can move towards the best universe randomly by wormholes.

All the above-mentioned terms can be modeled mathematically by adopting the roulette wheel mechanism. The universe can be arranged at each iteration for selecting white holes by use of the roulette wheel approach. From this perspective, this paper follows steps to deploy this algorithm effectively:

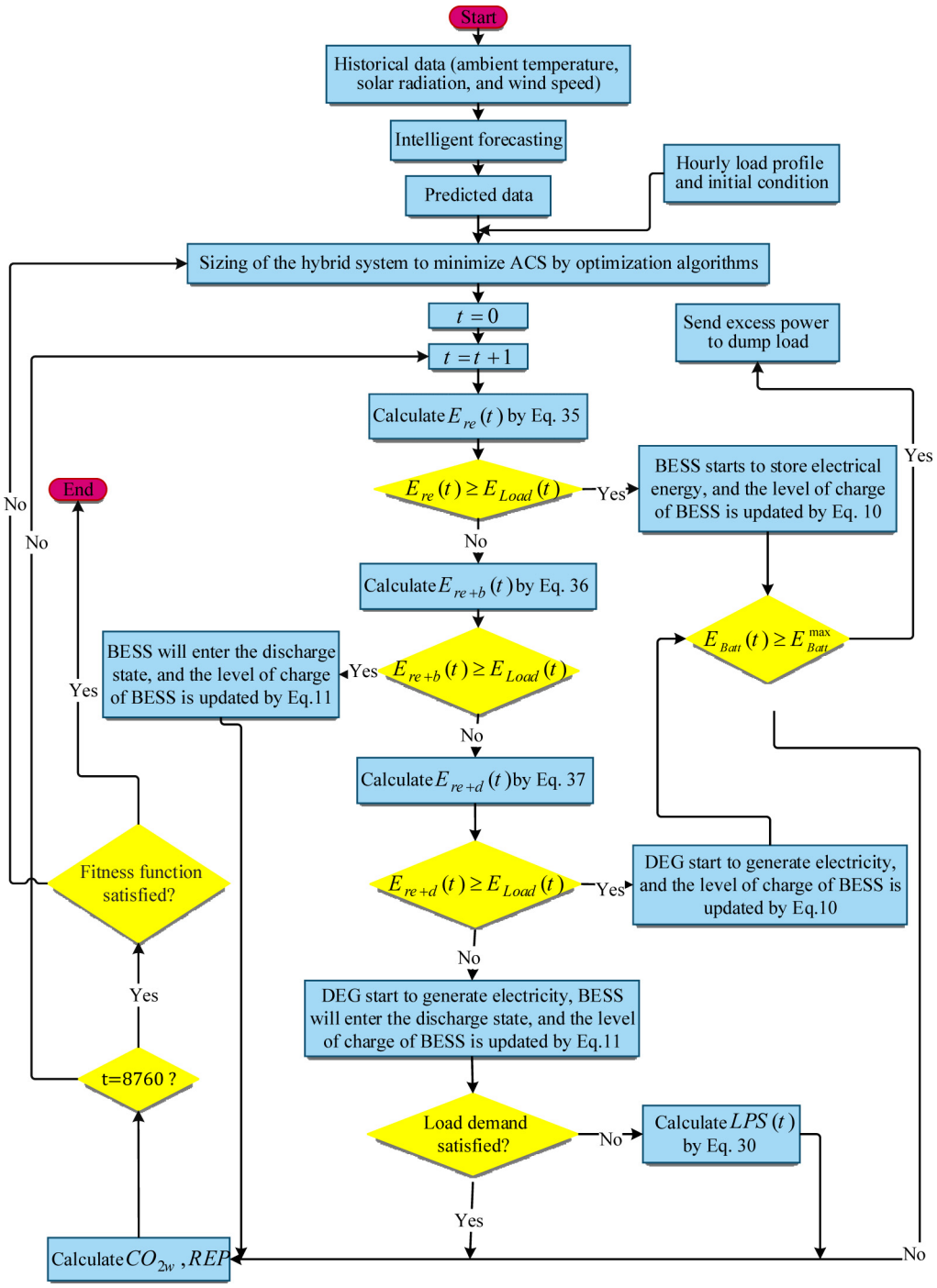

Fig. 2. Flowchart of the proposed energy management strategy.

Considering n and d as the number of universes and parameters, respectively, U matrix can be assumed as below:

$$U = \begin{pmatrix} x_1^1 & x_1^2 & \cdots & x_1^d \\ x_2^1 & x_2^2 & \cdots & x_2^d \\ \vdots & \vdots & \vdots & \vdots \\ x_n^1 & x_n^2 & \cdots & x_n^d \end{pmatrix} \tag{38}$$

The jth parameter of the ith the universe is calculated from the following equation:

$$x_i^j = \begin{cases} x_k^j & r_1 < NI\,(U_i) \\ x_i^j & r_1 \geq NI\,(U_i) \end{cases} \tag{39}$$

where, U_i is referred to as the ith universe and $NI\,(U_i)$ indicates the normalized inflation rate. In addition, r_1 is a random number in the range of 0 and 1.

The wormhole channels are fixed between a new and the best universe in order to keep the probability of enhancing the

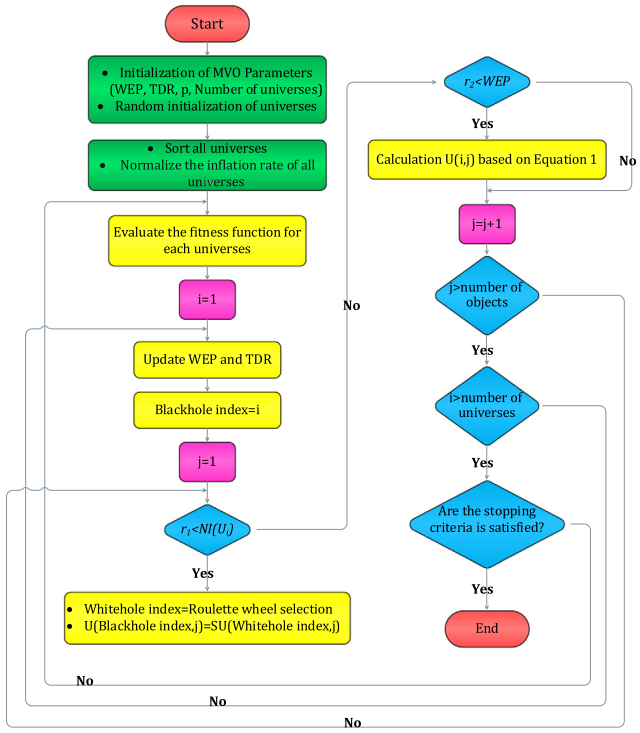

Fig. 3. Flowchart of multi-verse optimizer algorithm.

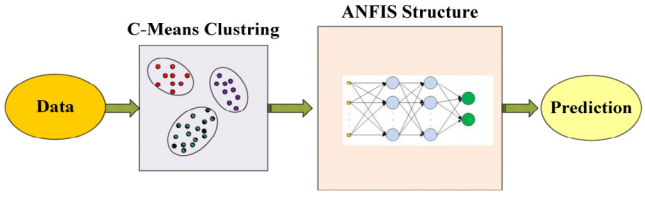

Fig. 4. Integration of fuzzy c-means clustering and ANFIS structure in weather forecasting.

inflation rate by the following equations:

$$x_i^j = \begin{cases} X_j + TDR \times \left(\left(ub_j - lb_j\right) \times r_4 + lb_j\right) & r_3 < 0.5 \\ X_j - TDR \times \left(\left(ub_j - lb_j\right) \times r_4 + lb_j\right) & r_3 \geq 0.5 \\ x_i^j & r_2 \geq WEP \end{cases}, \quad r_2 < WEP \tag{40}$$

where X_j is the jth parameter of the best universe, lb_j and ub_j are the lower and upper bounds of jth variable, and r_2, r_3 and r_4 are random numbers in the range of 0 and 1. In the following, an important factor, i.e. wormhole existence probability (WEP) is defined to increase linearly during the optimization process. Another important factor, traveling distance rate (TDR) is introduced to talk about the object which is deported by the wormhole to the best universe. WEP and TDR can be obtained by the following mathematical equations:

$$WEP = WEP_{min} + l \times \left(^{(WEP_{max} - WEP_{min})}/_{L}\right) \tag{41}$$

$$TDR = 1 - \left(^{l^{1/p}}/_{L^{1/p}}\right) \tag{42}$$

In Eqs. (36), (37), l and L are referred to as the current and maximum number of iterations, and p indicates the exploitation accuracy, which is assumed to be six in this study. In addition, the numerical value of WEP_{min} and WEP_{max} is 0.2 and 1, respectively. The flowchart of the MVO algorithm is illustrated in Fig. 3.

4.2. Iterative weather forecasting

Recently, renewable energies have brought many benefits to hybrid systems and consumers; however, RESs suffer from a crucial problem, i.e. dependency of their output power on the weather conditions, that is a time-variant and uncertain trend. One of the most effective approaches to address this concern is to propose an intelligent weather forecasting. It is often argued that two different methods can be deployed in case of weather forecasting, i.e., direct and iterative. In iterative forecasting, there is a single forecaster with one output node and predicted values will be defined as inputs for following forecasts. In contrary, in the direct forecasting, the number of output nodes are related to the forecast horizon period, and subsequent forecasts are directly obtained from forecast outputs. Broadly speaking, selection of iterative forecasting leads to negligible prediction errors, which may be created by various factors at the local and regional levels such as natural disasters and failure in meteorological devices; however, a direct forecasting often incurs significant rounding errors (Zhang et al., 2019).

Among existing iterative methods of weather prediction, the artificial neural network (ANN) has received a high level of consideration for different meteorological parameters. The main drawback of this iterative training method such as ANN is that as the number of inputs increases, the number of rules will also grow dramatically. Moreover, various meteorological events like floods, thunder and failures in devices can add noise and false data to the training process of the neural network. From this perspective, a pre-process clustering technique is proposed to remove outlier data and improve the performance of the neural network in case of forecasting.

Considering above concerns, we tried to address effects of various destructive factors indirectly by integration of (i) a Fuzzy C-Means (ANFIS-FCM) clustering technique, and (ii) Adaptive Neuro-Fuzzy Inference System, which is illustrated in Fig. 4, during our weather forecasting idea. In order to show how meteorological parameters can be estimated through iterative weather forecasting, fuzzy C-means is firstly introduced and the performance of ANFIS is described in the following sub-sections as follows:

4.2.1. Fuzzy c-means clustering

Fuzzy c-means (FCM) is a soft clustering method that allows existing data to move to specific clusters, with a degree specified by a membership grade. Unlike K-means methods, which are known to be a hard-clustering technique, the FCM algorithm is defined as a fuzzy mode of the K-means algorithm. This technique does not include sharp boundaries between different clusters and allows partial belongings of each data to various groups rather than a single group. In fuzzy C-means clustering, m vectors data $\{x_j, j = 1, 2, \ldots, m\}$ is divided into c cluster within three steps. In the first step, the centers of clusters $\{c_i, i = 1, 2, \ldots, c\}$ are randomly selected. In step-2, the membership matrix of each data point is calculated as follows (Abdulshahed et al., 2015b):

$$\mu_{ij} = {}^{1}/_{\sum_{k=1}^{c}\left(d_{ij}/d_{kj}\right)^{2/(q-1)}} \tag{43}$$

where μ_{ij} is referred to as the membership degree of data point j in cluster i, and q indicates the index of fuzziness fluctuating in the range $[1, \infty]$, and $d_{ij} = \left\|c_i - x_j\right\|$ is defined as the Euclidean distance between c_i and x_j. In the step-3, if the following objective function becomes lower than the specific lower limitation, this algorithm is stopped:

$$J\left(U, c_1, c_{2,\ldots,}c_c\right) = \sum_{i=1}^{c} J_i = \sum_{i=1}^{c} \cdot \sum_{i=1}^{c} \mu_{ij}^{q} d_{ij}^{2} \tag{44}$$

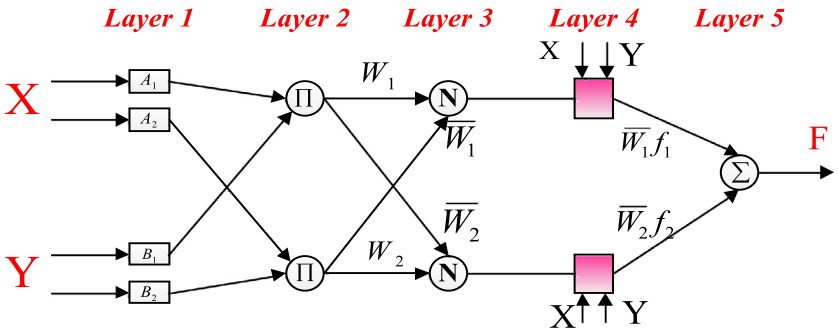

Fig. 5. The architecture of adaptive neuro-fuzzy inference system.

Finally, the following equation is deployed to obtain updated fuzzy cluster centers by this statement:

$$C_i = \left(\sum_{j=1}^{m} \mu_{ij}^{q} x_j\right) / \left(\sum_{j=1}^{m} \mu_{ij}^{q}\right) \tag{45}$$

In this paper, the FCM algorithm is deployed to separate our training data pairs into several uniform subsets, i.e., membership functions with different centers. In fact, several challenges in meteorological parameters such as failures in meteorological devices, floods and storms can be considered as outlier or noise data in this prediction process. In this regard, we firstly use this clustering technique to remove this data and afterward, the remaining data will be transferred to ANFIS section for learning process (Abdulshahed et al., 2015b).

4.2.2. Adaptive neuro-fuzzy inference system

In recent years, ANFIS has received a high level of consideration as a powerful modeling technique. This method is able to combine learning laws of ANN with fuzzy rule theory in the presence of the adaptive framework. In fuzzy logic theory, a fuzzy inference system (FIS) is defined as a well-known application where membership functions (MFs) of this application are defined based on trial and error. In this stage, ANN is able to determine parameters of MFs effectively to achieve an acceptable performance. Using the ANN method to develop the parameters of a fuzzy model allows the system to learn from a given set of training data. It is important to mention that the architecture of ANFIS, which contains five layers, includes several fixed and adaptive nodes. The layers of ANFIS architecture, which is shown in Fig. 5, are as follows:

In the first layer, the main purpose is to produce fuzzy values from input signals. This layer, which is often referred to as the fuzzification layer, converts input signals into fuzzy values which can be shown in the following statements:

$$O_{1,i=}\mu_{Ai}(X), \quad \text{for } i = 1, 2 \tag{46}$$

$$O_{1,i} = \mu_{Bi}(Y), \quad \text{for } i = 3, 4 \tag{47}$$

where the variables X and Y are considered as incoming signals. Other variables like i and 1 are symbols of the node and layer numbers, respectively. Furthermore, μ is referred to as the membership function which can be different shapes and $O_{i,1}$ is the output of each layer in this fuzzy process. The second layer is responsible for producing output from the multiplication of incoming fuzzy signals:

$$O_{2,i} = w_i = \mu_{Ai}(X) \times \mu_{Bi}(Y), \quad i = 1, 2 \tag{48}$$

In the third layer, the normalization of firing strengths from the previous layer is carried out accordingly:

$$O_{3,i} = \overline{w}_i = {}^{w_i}/_{(w_1+w_2)} \tag{49}$$

where $\overline{w}_i$ is the normalized firing strength parameter. In the following, the fourth layer is introduced as the defuzzification phase which can calculate defuzzification layers as follows:

$$O_{4,i} = \overline{w}_i f_i = \overline{w}_i (p_i X + q_i Y + r_i), \; i = 1, 2 \tag{50}$$

In the final phase, the last layer tries to calculate the overall output through summing incoming signals (Sabahi et al., 2009):

$$O_5 = \sum_i \overline{w}_i F_i = \left(\sum_i \overline{w}_i F_i\right) / \left(\sum_i \overline{w}_i\right) \tag{51}$$

This iterative weather forecasting is performed to provide future data according to two different stages. The first stage is related to offline training data and the second stage is presented to depict its online performance. At the first stage, historical day-ahead weather data related to previous years such as solar irradiation within a time interval is deployed to learn the proposed ANFIS system. When the training of ANFIS is done, the prediction of future meteorological parameters, e.g., radiation (W/m^2), temperature (°C) and wind speed (m/s) can be carried out using a previous learning stage. It is important to say that this prediction is carried out until the defined error becomes less than our intended threshold.

To depict the performance of our proposed method in comparison with ANN and radial basis function (RBF) methods, predicted results of solar radiation, ambient temperature, and wind speed for the last week of the previous year are shown in Figs. 6, 7, and 8, respectively. It is clear that ANFIS-FCM method is able to track historical data with the least amount of error that confirms the superiority of this prediction method for meteorological parameters used in our hybrid systems. This amount of small deviation between real data and proposed method is a result of combination of FCM and ANFIS that can decrease outlier historical data considerably.

Besides, Table 1 provides information about several criteria such as mean square error (MSE), root mean square error (RMSE), mean of error, standard deviation (STD) of error, that confirms ANFIS-FCM has a lower error compared to the mentioned methods.

Table 1
Error comparison of different weather forecasting methods.

	Methods	MSE	RMSE	Mean of error	STD of error
Solar radiation	ANN	0.00542	0.07363	−0.00585	0.07340
	RBF	0.00590	0.07680	−0.00129	0.07680
	ANFIS-FCM	0.00388	0.06227	0.00099	0.06226
Temperature	ANN	1.15622	1.07528	0.01597	1.07522
	RBF	5.98207	2.44583	−0.04771	2.44550
	ANFIS-FCM	0.82973	0.91089	−0.01531	0.91082
Wind speed	ANN	2.82199	1.67988	−0.06386	1.67990
	RBF	4.13170	2.03266	−0.20817	2.03177
	ANFIS-FCM	2.66197	1.63155	−0.01538	1.61831

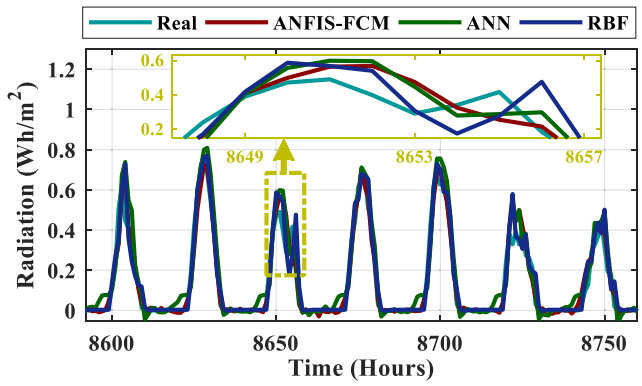

Fig. 6. Prediction of solar radiation data.

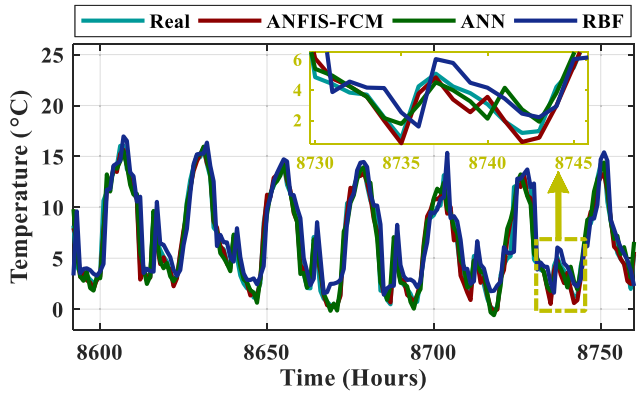

Fig. 7. Prediction of ambient temperature data.

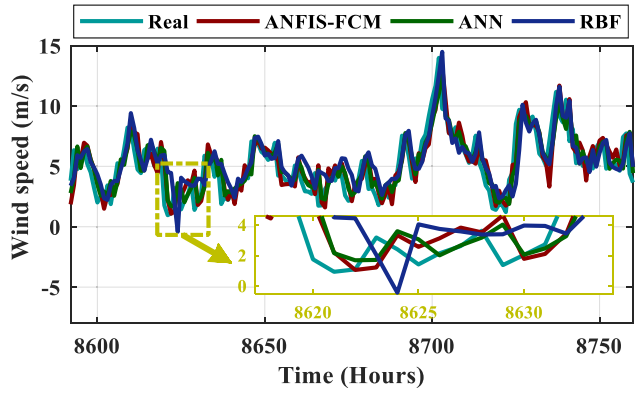

Fig. 8. Prediction of wind speed data.

5. Simulation results and discussion

5.1. Assessment of the best meta-heuristic method

In this study, after obtaining the weather forecasting information, which was presented in the previous section, the profile of load is illustrated in Fig. 9. Three hybrid energy scenarios, including PV/WTG/BESS/DEG, WTG/BESS/DEG, and PV/BESS/DEG considering both REP and LSPS criteria are evaluated and the results from optimization tools are given during the combination of renewable energy sources in different diagrams. Several meta-heuristic algorithms are deployed to minimize the annualized cost of the system and satisfy $LPSP_{max}$ and REP_{min}. The parameters of the hybrid system and coefficients of meta-heuristic

Table 2
The parameters of the hybrid system related to this project.

Project parameters		Battery [5, 20, 27]	
i (%)	5	S^{rat}_{Batt} (kWh)	1.3
f (%)	2	*Voltage* (V)	12
Lifetime (Year)	20	σ	0.0002
PV panel [5, 20, 27]		*DOD*	0.8
P^{rat}_{PV} (kW)	0.12	η_{Batt} (%)	85
α	−0.0037	$E^{initial}_{Batt}$ (%)	80
NOCT	33	*CapitalCost*($)	130
T_{ref} (°C)	25	*O&MCost* ($/year)	0
I^{ref} (W/m^2)	1000	*Lifespan* (year)	5
η (%)	12	Diesel engine generator [4, 18]	
CapitalCost ($)	614	P^{rat}_{DEG} (kW)	1.8
O&MCost ($/year)	0	A_{DEG}	0.2461
Lifespan (year)	20	B_{DEG}	0.08145
Wind turbine generator[3, 5, 20, 27]		*CapitalCost* ($)	550
P^{rat}_{WTG} (kW)	1	*O&MCost* ($/h)	0.144
v_{cut-in} ($\frac{m}{s}$)	2.5	*Lifespan* (h)	15 000
$v_{cut-out}$ ($\frac{m}{s}$)	13	P_{fuel}($/l)	1.18
v_r ($\frac{m}{s}$)	11	Inverter/ Converter [20, 27]	
H (m)	20	$P^{rat}_{inv/conv}$ (kW)	3
α	0.25	η_{Inv} (%)	95
CapitalCost ($)	3200	*CapitalCost* ($)	2000
O&MCost ($/year)	100	*O&MCost* ($/year)	0
Lifespan (year)	20	*Lifespan* (year)	10

Table 3
Defined parameters of all meta-heuristic algorithms.

Parameters of optimization			
N_{run}	30	*Iteration*	1000
N^{max}_{PV}	1500	N^{max}_{WTG}	500
N^{max}_{Batt}	1500	N^{max}_{DEG}	50
MVO		GOA	
Universes	100	*Searchagents*	100
WEP_{max}	1	C_{max}	1
WEP_{min}	0.2	C_{min}	0.00001
p	6	f	0.5
DA		l	1.5
Searchagents	100	SSA	
C_{max}	0.9	*Searchagents*	100
C_{min}	0.5	GWO	
β	1.5	*Searchagents*	100

algorithms have been given in Tables 2 and 3, respectively. The maximum and minimum bounds of decision variables for WTG change from 0 to 500, for PV varies from 0 to 1500, for the battery is a range from 0 to 1500 and for DEG is a range from 0 to 50. At the first step, it is supposed that the state of charge of batteries is 80% of the nominal value. The results of different optimization tools for PV/WTG/BESS/DEG system are listed in Table 4, and different criteria including maximum, minimum, mean, and standard deviation of the annualized cost of the system have been recorded over 30 independent runs of each algorithm, along with various loss of power supply probability ($LPSP_{max}$) and different renewable energy penetration (REP_{min}). Moreover, the rank of each algorithm is shown in order to compare the assumed meta-heuristic algorithms in terms of different criteria.

Table 4 compares the performance of different meta-heuristic algorithms. It can be observed that multi-verse optimizer delivers the best performance over 30 runs. In this combination, all distributed generations, namely, PV/WTG/BESS/DEG participate practically. It is important to mention that during the implementation of this site, one of the main objectives is to deploy renewable energy sources considering their maximum potential

Table 4
Defined parameters of all meta-heuristic algorithms.

Optimization algorithm	Parameters	*ACS* ($)										Rank
		$LPSP_{max}$ (%)									Average	
		0	1	3	5	10	1	1	1	1		
		REP_{min} (%)										
		95	95	95	95	95	91	93	97	100		
DA	Min	57 788.1	54 785.7	52 616.3	50 173.4	45 968.1	53 495.2	53 936.0	56 587.5	65 954.2	54 589.4	4
	Max	58 333.2	62 198.3	52 816.8	50 538.6	51 464.4	53 686.3	60 158.5	57 374.7	66 623.6	57 021.6	4
	Mean	57 993.0	56 408.1	52 719.0	50 303.3	47 146.7	53 571.5	55 277.8	56 930.5	66 160.8	55 167.9	4
	STD	227.2	2395.3	91.8	154.9	2415.1	79.2	2733.7	288.3	270.0	961.7	4
GOA	Min	57 551.0	54 785.7	52 632.0	50 185.6	45 285.4	53 495.2	53 946.6	56 846.3	66 006.4	54 526.0	3
	Max	62 223.8	69 767.8	69 223.4	50 428.2	45 626.8	53 751.8	54 011.4	57 978.1	82 120.4	60 570.2	5
	Mean	58 302.5	55 760.4	56 046.0	50 352.2	45 482.8	53 619.0	53 964.9	57 300.1	78 103.3	56 547.9	5
	STD	972.9	2791.6	7367.8	106.0	153.3	100.2	26.3	439.3	6790.9	2083.1	5
GWO	Min	58 969.4	54 785.7	52 616.3	50 156.7	45 262.8	53 624.6	54 555.0	56 571.9	65 919.1	54 717.9	5
	Max	59 120.7	54 805.2	52 632.0	50 185.6	45 965.1	53 702.0	54 562.5	56 587.5	65 933.1	54 832.6	3
	Mean	59 017.1	54 794.2	52 619.4	50 169.1	45 403.2	53 666.4	54 556.5	56 578.5	65 921.9	54 747.4	3
	STD	64.7	8.4	7.0	12.4	314.1	39.0	3.4	7.5	6.3	51.4	2
SSA	Min	57 569.6	54 785.7	52 616.3	50 156.7	45 262.8	53 443.2	53 936.0	56 571.9	65 919.1	54 473.5	2
	Max	58 481.3	55 075.7	52 630.7	50 259.8	45 287.6	53 706.5	53 941.8	57 271.0	65 946.8	54 733.5	2
	Mean	57 930.2	54 797.9	52 622.0	50 195.9	45 277.4	53 567.0	53 940.6	56 734.8	65 934.5	54 555.6	2
	STD	230.4	81.6	7.9	43.9	10.4	120.1	2.6	303.5	12.0	90.3	3
MVO	Min	57 509.3	54 785.7	52 379.8	50 156.7	45 262.8	53 416.7	53 936.0	56 482.5	65 919.1	54 427.6	1
	Max	57 890.0	54 801.6	52 393.9	50 200.6	45 280.0	53 505.4	53 965.6	56 494.2	65 991.9	54 502.6	1
	Mean	57 653.7	54 740.5	52 382.6	50 165.4	45 270.1	53 437.3	53 946.0	56 484.8	65 944.7	54 447.2	1
	STD	93.4	41.1	6.3	19.6	6.2	38.6	11.4	5.2	19.1	26.8	1

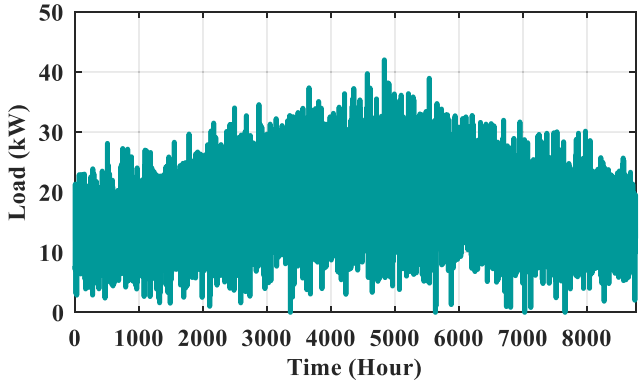

Fig. 9. Hourly load profile for one year (8760 h).

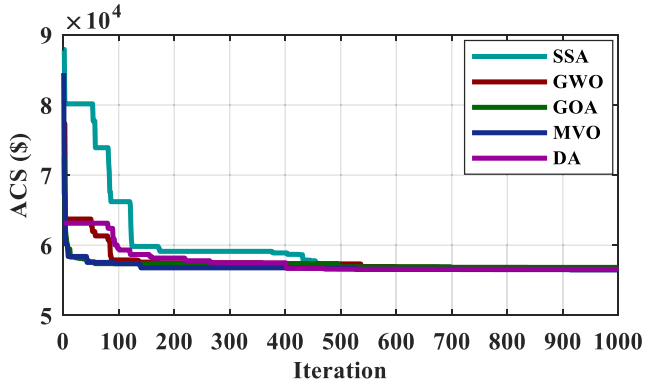

Fig. 10. Convergence characteristics of different meta-heuristic algorithms SSA, GWO, GOA, MVO, and DA at $LPSP_{max}$ = 1%, REP_{min} = 97% (Strategy: PV/WTG/BESS/DEG).

owing to financial issues as well as the debilitated road network of this province in Iran. From this perspective, the amount of penetration of renewable energy production changes from 91% to 100% in order to deploy the highest capacity of existing PV, WTG, and battery banks. Using DEG, as an ancillary source of energy generation in this area, can be beneficial. This generation unit helps the hybrid systems to minimize the annualized cost of the system in a realistic way, although the DEG backup generation unit is not considered as an independent energy production source due to the high price of fuel and the lifetime of DEG. In addition, based on data given in Table 4, the amount of $LPSP_{max}$ varies from 0% to 10% in order to guarantee the reliability of the system in this remote area. To indicate the performance of each algorithm and select the best optimizer among suggested ones, the rank of each algorithm, which varies from 5 to 1 with regard to a desirable operation of each algorithm, is defined based on the average standard. This important standard, i.e. Average, states the mean value of 9 obtained results for each index. When all mentioned algorithms are compared on this economic sizing for different values of $LPSP_{max}$ and REP_{min}, MVO delivers the best performance in terms of the average of the minimum ($54 427.6), an average of the maximum ($54 502.6), an average of the mean ($54 447.2) as well as an average of the standard deviation ($26.8) of the annualized cost of the system (ACS). It can be observed that the difference between the average of the maximum and the minimum annualized cost of the system for the MVO algorithm is $75, which is lower than other algorithms, i.e. DA, GOA, GWO, and SSA. Another index, the standard deviation for two algorithms including GOA and DA, is not acceptable compared to other optimization methods. As it can be observed, MVO has achieved the best rank in four indexes, while GOA is not able to show a good performance based on its ranks in all sections. Based on this average parameter, MVO yields the least amount compared to other algorithms which depict that deploying this algorithm is an appropriate selection for sizing a hybrid system in this province.

As a proper example, the convergence process of mentioned meta-heuristic algorithms has been illustrated in Fig. 10 to resolve this economic sizing at the 1000 iteration number for the best solution. Based on this diagram, MVO presents a promising performance in terms of convergence speed and the best solution compared to other mentioned optimization algorithms.

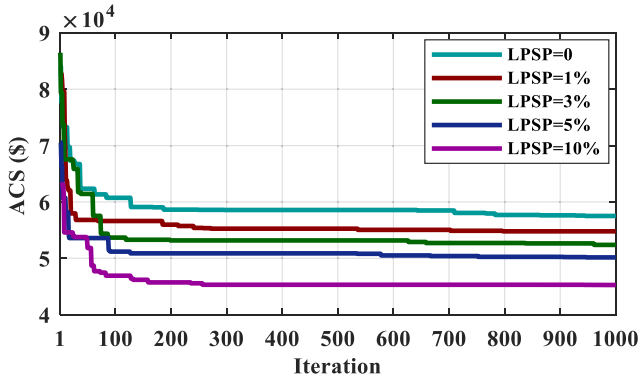

Fig. 11. Convergence trend of the multi-verse optimizer (MVO) at different $LPSP_{max}$ and REP_{min} = 95% (Strategy: PV/WTG/BESS/DEG).

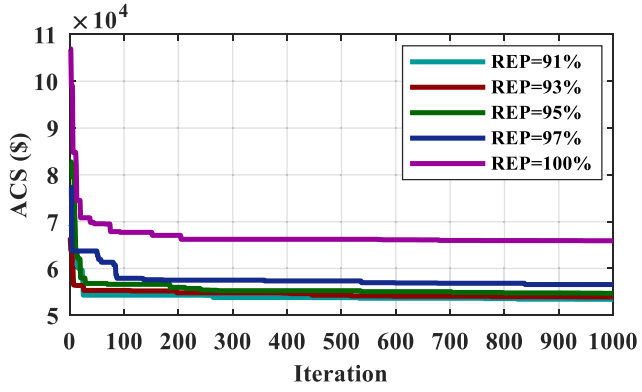

Fig. 12. Convergence trend of the multi-verse optimizer (MVO) at different REP_{min} and $LPSP_{max}$ = 1% (Strategy: PV/WTG/BESS/DEG).

5.2. Different LPSP versus REP for different proposed scenarios

In the following, a comparison between different $LPSP_{max}$ ($LPSP_{max}$ = 0 means the highest level of reliability without blackout) is made at REP_{min} = 95% to depict the acceptable convergence speed of the MVO meta-heuristic algorithm. According to Fig. 11, it can be observed that the main purpose of this algorithm is to achieve a balance between the level of reliability and the annualized cost of the system. It is often argued that when the reliability of the system decreases, the annualized cost of the system experiences a downward trend.

For PV/WTG/BESS/DEG contribution, the amount of reliability is defined at $LPSP_{max}$ = 1% and the penetration of RES contribution is considered at REP_{min} = 91%, 93%, 95%, 97%, and 100%. As it can be concluded from Fig. 12, using renewable energy sources can contribute to an increasing trend in the annualized cost of the system. In this local area, when consumers take advantage of DEG as an ancillary unit, the total cost decreases considerably compared to deploying DEG as a main power generation unit. Using DEG as a backup generation unit along with RESs such as wind turbine, PV, and battery bank can result in decline in the annualized cost of the hybrid system. Finally, Fig. 13 illustrates the effect of $LPSP_{max}$ on the annualized cost of the system for different contributions of renewable energy sources.

Based on the obtained results in Table 4, the MVO algorithm is selected as the best algorithm in this study. In the following, Table 5 depicts the optimum number of each power generation unit for a contribution of PV/WTG/BESS/DEG and the annualized cost of the system considering different $LPSP_{max}$ and REP_{min} criteria. In this table, the amount of fuel consumption for DEG, as a backup

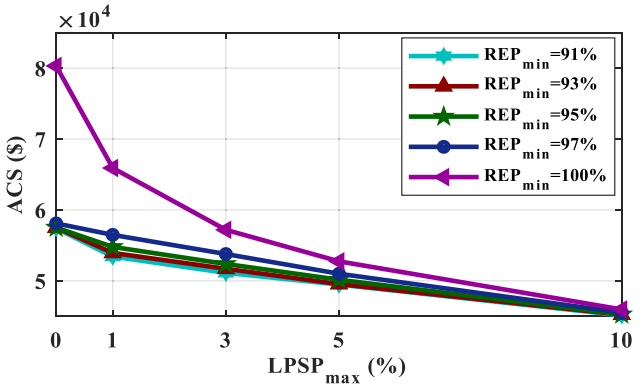

Fig. 13. The impact of $LPSP_{max}$ on the annualized cost of the system in different renewable energy penetration levels (Strategy: PV/WTG/BESS/DEG).

generation unit, and the amount of excess power, which is generated during each scenario, is shown. According to the obtained results, when $LPSP_{max}$ is set at 10% and the minimum amount of *REP* is defined at 95%, the minimum annualized cost of the system is $45 262.78. In this case, the optimum sizing is N_{PV} = 336, N_{WTG} = 45, N_{Batt} = 204, and N_{DEG} = 2. It can be observed that DEG along with other RESs yields more satisfactory performance. In the following, Tables 6 and 7 present the figures related to two contributions of RESs, namely, PV/BESS/DEG and WTG/BESS/DEG. According to these mentioned tables, PV/WTG/BESS/DEG is the best choice in terms of minimizing the annualized cost of the system, so that the cost item of PV/WTG/BESS/DEG contribution for a different level of *LPSP* and *REP* is lower than two assumed contributions.

5.3. The annualized cost of system for different proposed scenarios

Fig. 14 shows the annualized cost of the system for three different contributions of RESs in this hybrid system. It can be observed that the intelligent combination of PV/WTG/BESS/DEG delivers the most promising performance during various LPSP, which varies from 0% to 10%. Moreover, the amount of renewable energy penetration remains stable at 95%. In the next step, Fig. 15 illustrates this total annualized cost when $LPSP_{max}$ is 1% and REP_{min} changes from 91% to 100%. From this figure, it can be concluded that an intelligent combination of PV/WTG/BESS/DEG is able to achieve an acceptable balance between ACS ($) and REP. During other contributions of RESs, namely, PV/BESS/DEG and WTG/BESS/DEG, the lack of one of RESs will lead DEG to compensate for the load demand, which results in a noticeable reduction in the lifetime of DEG. Due to the weak road network and the high price of petrol in this remote area, the annualized cost of the system will experience an ever-increasing trend. In addition, based on the geographical location of this area, wind turbine experiences a broad range of changes in output power compared to solar panels, which tend to change slightly. As a result, in the strategy of WTG/BESS/DEG, a higher level of excess power is obtained. For example, excess power generation, when $LPSP_{max}$ is 1% and REP_{min} changes from 91% to 100%, have been shown in Fig. 16. It is important to mention that during the best contribution of RESs, PV/WTG/BESS/DEG, MVO tries to minimize the consumption rate of DEG fuel compared to other proposed contributions and regards DEG as a cost-effective power generation unit based on Fig. 17.

Finally, Fig. 18 depicts the breakdown of different costs, i.e. the costs related to PV cell, wind turbine, battery, inverter, and DEG

Table 5
The summary of obtained results by MVO algorithm in PV/WTG/BESS/DEG contribution.

$LPSP_{max}$ (%)	REP_{min} (%)	N_{PV}	N_{WTG}	N_{Batt}	N_{DEG}	$LPSP$ (%)	REP (%)	ACS ($)	Fuel consumption (Liter/year)	Excess power generation (kW/year)
0	95	424	45	263	14	0.0000	95.6934	57 509.31	5904.98	22 113.95
1	95	451	44	275	7	0.9681	95.0030	54 785.71	3114.90	18 527.93
3	95	446	42	236	5	2.7791	95.0218	52 379.78	3019.12	17 155.33
5	95	405	44	259	3	4.9996	96.3106	50 156.67	1997.08	13 138.93
10	95	336	45	204	2	9.9964	95.9042	45 262.78	2065.49	10 860.09
1	91	359	46	233	8	1.0000	91.8157	53 416.71	5701.52	13 255.60
1	93	379	47	239	8	0.8815	93.0236	53 935.96	4911.49	15 969.97
1	97	492	44	319	6	0.9929	97.0233	56 482.48	1906.06	22 252.71
1	100	635	52	374	0	0.9981	100.0000	65 919.10	0.00	57 506.03

Table 6
The summary of obtained results by MVO algorithm in PV/BESS/DEG contribution.

$LPSP_{max}$ (%)	REP_{min} (%)	N_{PV}	N_{WTG}	N_{Batt}	N_{DEG}	$LPSP$ (%)	REP (%)	ACS ($)	Fuel consumption (Liter/year)	Excess power generation (kW/year)
0	95	879	0	316	15	0.0000	95.3355	65 956.38	6514.16	27 511.01
1	95	860	0	342	8	0.9916	95.1305	62 036.54	3826.40	17 160.72
3	95	858	0	348	5	2.9933	95.8761	60 015.05	2501.55	15 822.47
5	95	805	0	339	4	4.9882	95.4459	57 013.72	2624.70	9672.13
10	95	758	0	299	2	9.9769	96.6659	51 464.45	1783.51	6693.29
1	91	770	0	302	9	0.9952	92.3658	60 024.17	6751.52	10 050.89
1	93	787	0	306	9	0.9315	93.0497	60 146.70	6253.59	11 447.94
1	97	920	0	417	7	0.9783	97.0050	64 847.08	2182.09	22 830.57
1	100	1083	0	638	0	0.9971	100.000	77 676.06	0.00	46 045.90

Table 7
The summary of obtained results by MVO algorithm in WTG/BESS/DEG contribution.

$LPSP_{max}$ (%)	REP_{min} (%)	N_{PV}	N_{WTG}	N_{Batt}	N_{DEG}	$LPSP$ (%)	REP (%)	ACS ($)	Fuel consumption (Liter/year)	Excess power generation (kW/year)
0	95	0	102	446	14	0.0000	95.0839	66 739.79	7087.64	37 207.20
1	95	0	109	504	7	0.9863	95.5823	64 906.01	3119.06	38 251.86
3	95	0	101	476	5	2.9907	95.3553	60 910.55	3045.89	27 911.25
5	95	0	99	402	4	4.9987	95.4106	57 293.25	2948.32	27 957.12
10	95	0	95	325	2	9.9981	96.2760	51 640.03	1951.27	26 740.12
1	91	0	95	325	9	0.8204	91.0048	60 040.32	7479.68	29 109.88
1	93	0	102	388	8	0.9949	93.0711	61 622.86	5201.81	33 626.80
1	97	0	114	600	7	0.6802	97.0011	68 639.57	2182.09	42 842.79
1	100	0	134	945	0	0.9995	100.0000	84 556.65	0.00	69 504.79

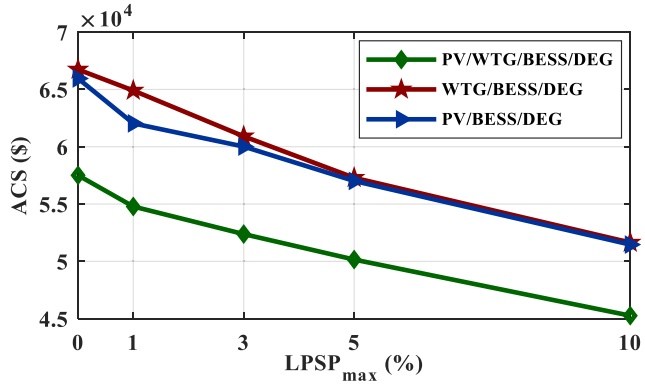

Fig. 14. The annualized cost of the system of three different contributions for various $LPSP_{max}$ and $REP_{min} = 95\%$.

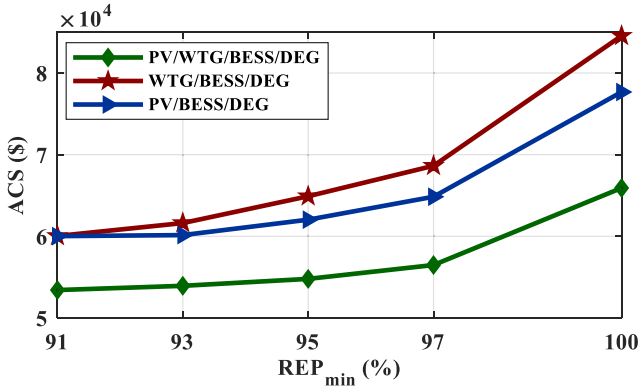

Fig. 15. The annualized cost of the system of three different contributions for various REP_{min} and $LPSP_{max} = 1\%$.

for different levels of reliability. Based on this figure, which is associated with PV/WTG/BESS/DEG contribution, the maximum cost belongs to PV production. The main reason is that in this area due to special weather conditions and extra exiting sunny days, PV plays an active role in meeting consumer's requirements. In the following, Fig. 19 shows another breakdown of produced energy by different amounts of renewable energy penetration. It can be observed from Fig. 19 that by increasing the penetration of RESs in this hybrid system, the generated power of DEG decreases, and the penetration level of PV in energy production experience an increasing trend from 28% to 39%.

5.4. An overview of power generated by PV/WTG/BESS/DEG

In the next step, to investigate the performance of PV, wind turbine, battery, and DEG during power generation schedule and satisfying requirements of consumers in a sensible way, a real pattern of load in kW can be given in Fig. 20. The time interval is regarded for a specific week from 1th to 7th January which includes 168 h of total consumption through local people.

It can be observed from Figs. 21 and 22 that when the level of RES penetration increases from 91% to 100% at $LPSP_{max} = 1\%$, the

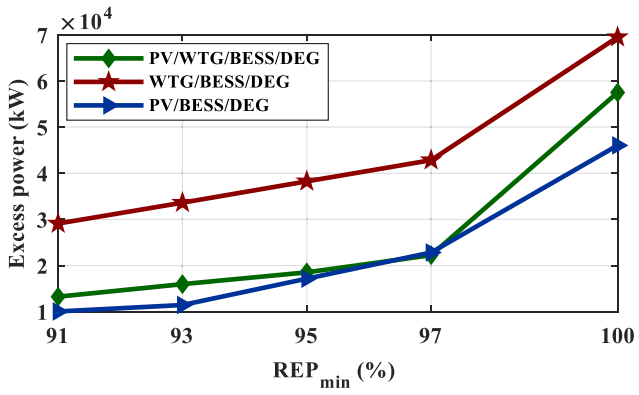

Fig. 16. Excess power generation of three different contributions for various $REP_{\min}$ and $LPSP_{\max} = 1\%$ over a year.

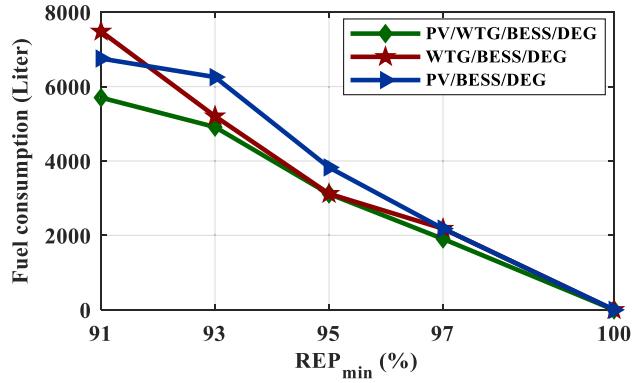

Fig. 17. Fuel consumption of DEG of three different contributions for various $REP_{\min}$ and $LPSP_{\max} = 1\%$ over a year.

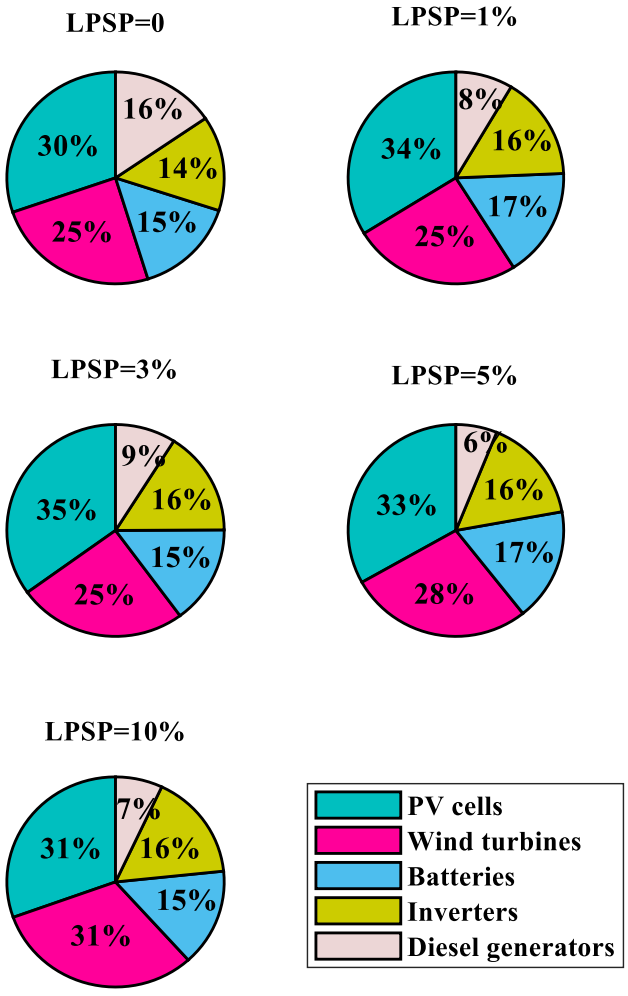

Fig. 18. Breakdown of the annualized cost of the system for a different level of reliability and $REP_{\min} = 95\%$ over a year.

amount of PV energy production will increase. During the contribution of PV/WTG/BESS/DEG in this hybrid system, this amount of generated PV power is lower than when the contribution is PV/BESS/DEG. The main reason is that during PV/WTG/BESS/DEG contribution, WTG is responsible for providing a penetration of energy production based on the geographical location of this remote area, although the contribution of wind turbine generators in this project is lower than that of solar panels owing to an existing desert in this area. In the following, Figs. 23 and 24 have been illustrated for different contributions to depict the amount of WTG energy production. As it can be observed, in the presence of PV contribution, WTG produces less energy compared to when there is no PV contribution. When the PV generation faces a drop, WTG has to play an active role in providing consumer's demand.

In the next stage, the amount of energy, which is produced by DEG, is shown in Figs. 25, 26, and 27, respectively, when the renewable energy penetration varies from 91% to 100%. It is important to mention that when REP_{min} is 100%, all consumers' requirement is provided by renewable energy sources including PV, WTG, and battery which results in increasing annualized cost of this hybrid system.

In the final stage, the behavior of the battery for three different contributions has been shown in Figs. 28, 29, and 30. Based on the obtained patterns, during PV/WTG/BESS/DEG contribution, BESS delivers the best performance in terms of the amount of repetition of charge and discharge process and slight variations compared to other contributions, namely, PV/BESS/DEG and WTG/BESS/DEG. It should be noted that severe changes in the charge and discharge processes could contribute to reduction in the lifetime and performance of BESS.

5.5. A case study: A pattern of power generation during a specific time interval

In this section, the performance of each power generation unit is evaluated, and a pattern of power generation scheme, which is distributed by the MVO algorithm at $LPSP_{max} = 3\%$, $REP_{min} = 95\%$, is depicted in Fig. 31. In order to illustrate the capability and flexibility of the proposed energy management strategy in case of different values of LPSP, the value of $LPSP_{max}$ is considered to be 3% in this case study. This figure includes the level of produced energy by WTG and PV, along with the load demand in kW. To indicate the performance of this proposed strategy, this period of time (1st to 2nd January) is divided into four distinct parts. In the first time interval (from 33 to 40 h), all loads are supplied by PV and WTG power generation units, and the additional produced power is used to charge the battery bank up to the maximum permissible bound. In the second time interval (1–13, 16, 32, 41–46 h), renewable energy sources are not able to supply all load demand. As a result, such deficiency is compensated by the battery bank. In the third period of time, (14–15, 17–19, 23–27, 30–31, 47–48), the load is fully supplied by deploying the diesel engine generator, PV, WTG, and battery. In the final time interval (20–22, 24–26, 28–29 h), total power which is generated

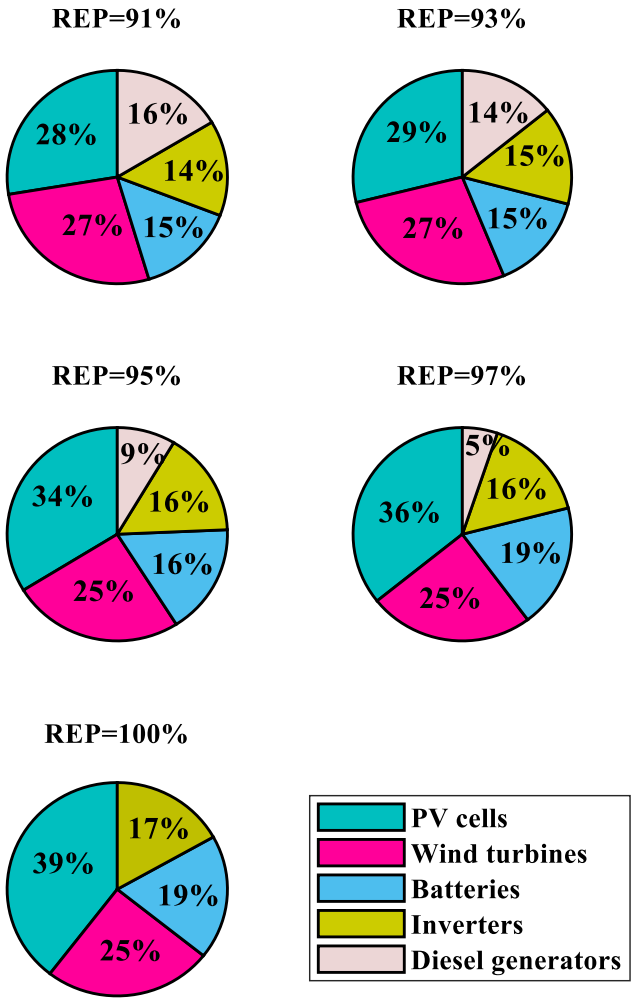

Fig. 19. Breakdown of the annualized cost of the system for a different level of renewable energy penetration and $LPSP_{max} = 1\%$ over a year.

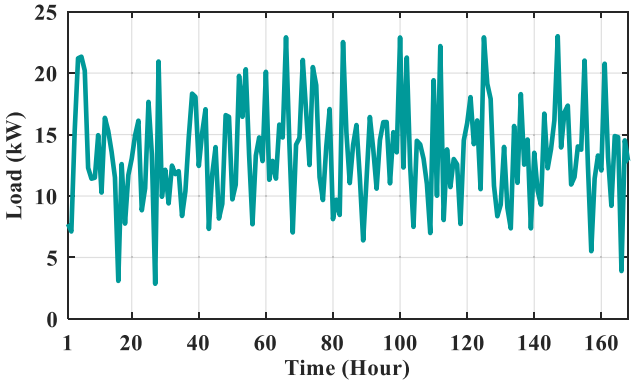

Fig. 20. The real pattern of load in kW from 1st to 7th January (168 h).

by PV, WTG, DEG, and battery bank considering the minimum permissible discharge are not able to supply all the loads. As a result, some portions of the load cannot be supplied and the concept of loss of power supply based on (28) will occur. For more details, the behavior of the battery bank and the state of charge of this bank are depicted in Fig. 32.

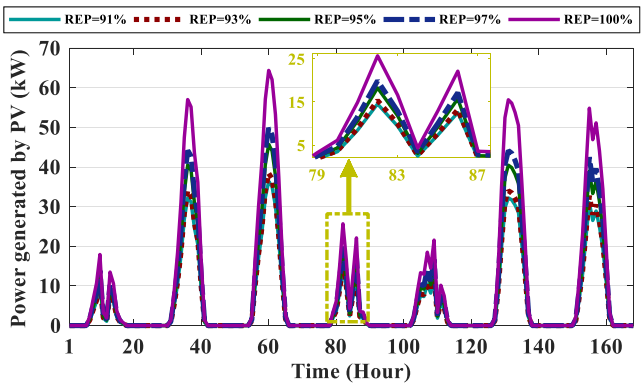

Fig. 21. The power generated by PV from **1st** to **7th** January for PV/WTG/BESS/DEG strategy at $LPSP_{max} = 1\%$.

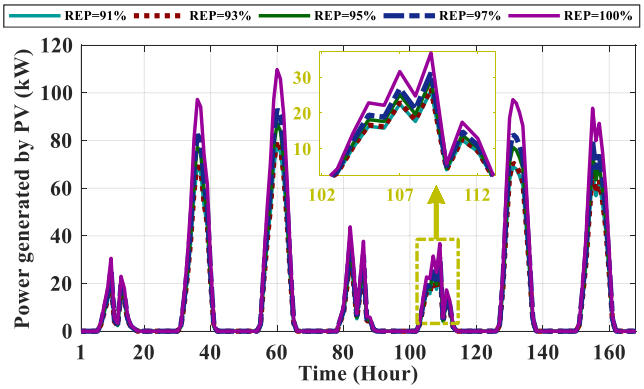

Fig. 22. The power generated by from 1st to 7th January for PV/BESS/DEG strategy at $LPSP_{max} = 1\%$.

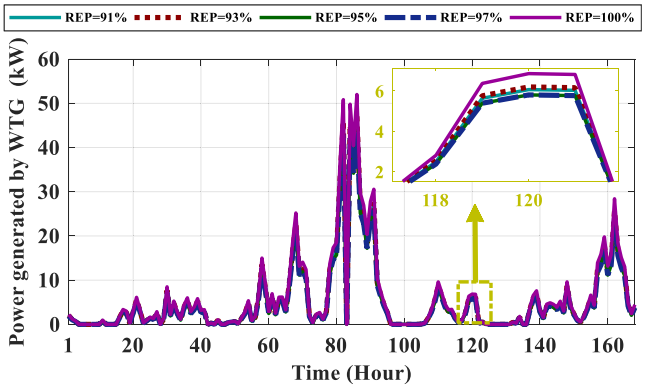

Fig. 23. The power generated by WTG from 1st to 7th January for PV/WTG/BESS/DEG strategy at $LPSP_{max} = 1\%$.

5.6. CO_2 emission

The mass of CO_2 gas, which is produced by diesel engine generators, is illustrated in Table 8 with various $LPSP_{max}$ and REP_{min} values in the presence of different configurations. Based on the obtained results from the mentioned table, as the REP_{min} increases, the share of diesel engine generators from total produced power experiences a downward trend resulting in reduction of carbon emission. Table 8 shows that the hybrid system can significantly reduce pollutant gases emission. This phenomenon is specifically evident in the reduction of carbon dioxide. For instance, PV/WTG/BESS/DEG hybrid configuration is able to save

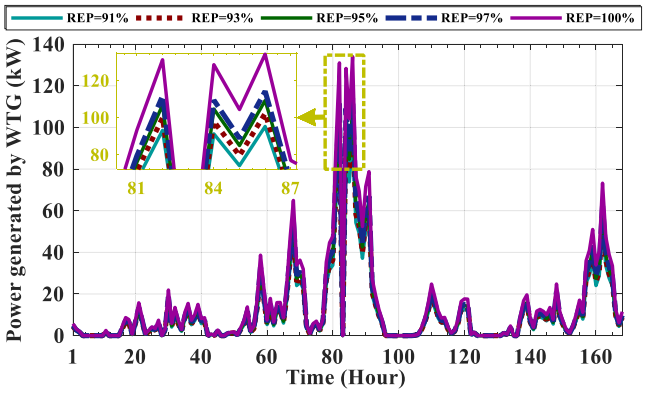

Fig. 24. The power generated by WTG from 1st to 7th January for WTG/BESS/DEG strategy at $LPSP_{max} = 1\%$.

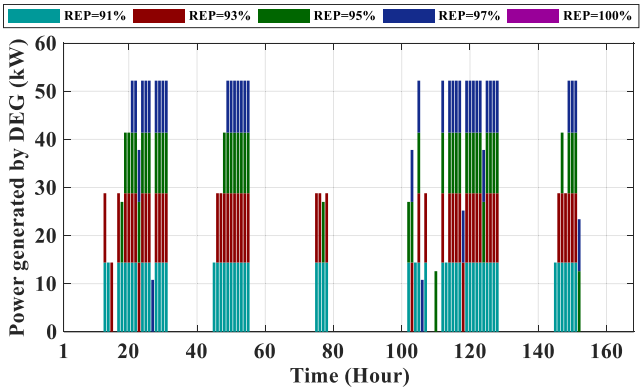

Fig. 25. The power generated by DEG every hour from 1st to 7th January for PV/WTG/BESS/DEG strategy at $LPSP_{max} = 1\%$.

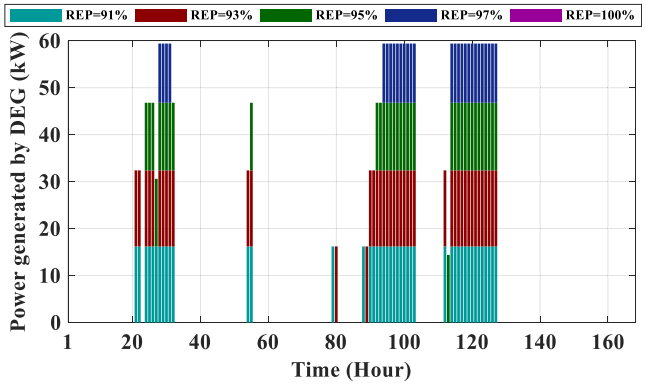

Fig. 26. The power generated by DEG every hour from 1st to 7th January for PV/BESS/DEG strategy at $LPSP_{max} = 1\%$.

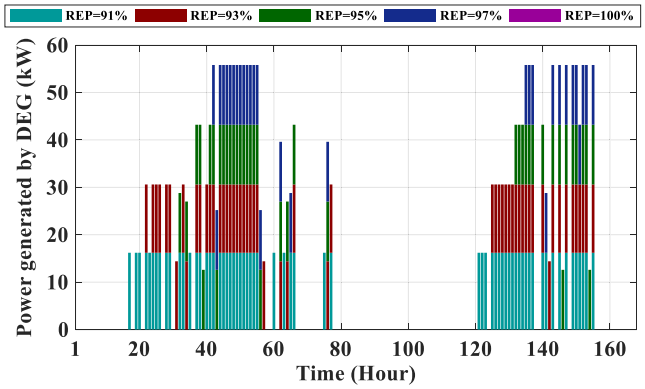

Fig. 27. The power generated by DEG every hour from 1st to 7th January for WTG/BESS/DEG strategy at $LPSP_{max} = 1\%$.

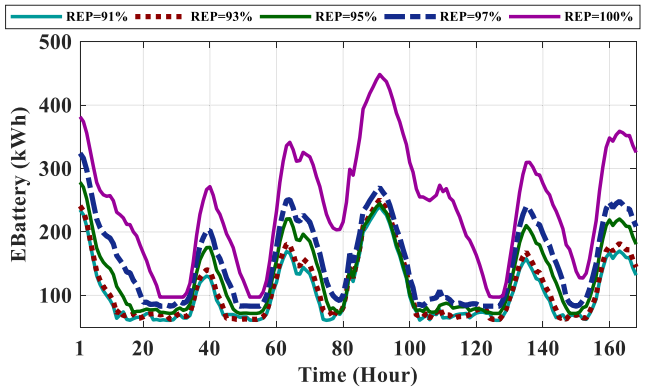

Fig. 28. Amount of stored energy in BESSs from 1st to 7th January for PV/WTG/BESS/DEG strategy at $LPSP_{max} = 1\%$.

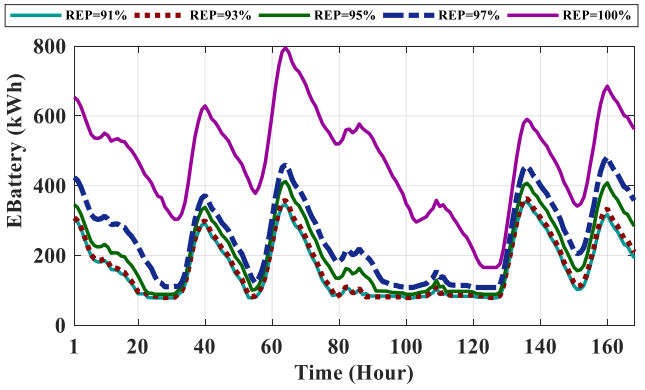

Fig. 29. Amount of stored energy in BESSs from 1st to 7th January for PV/BESS/DEG strategy at $LPSP_{max} = 1\%$.

96.13% of CO_2 emission compared to DEG system at $REP_{min} = 97\%$ and $LPSP_{max} = 1\%$.

5.7. Sensitivity analysis

5.7.1. Wind speed and solar radiation

The results of the wind speed and solar radiation sensitivity analysis for the PV/WTG/BESS/DEG hybrid system with $LPSP_{max} = 1\%$ and different REP_{min} values are shown in Figs. 33 and 34, respectively. According to the obtained results from Fig. 33, it is clear that as the wind speed has increased, the optimal number of wind turbine generators and consequently the share of wind turbines in the annual cost of the system has increased. However, the optimal number of PV and the share of them has decreased from ACS. For instance, at $REP_{min} = 91\%$, the 40% increment of wind speed (from −20% to + 20% real wind speed), has caused the optimal number of wind turbines to increase from 6 to 52. While this trend has caused the optimal number of PV, batteries, and diesel to drop from 704, 281, and 9 to 211, 223, and 8, respectively. Moreover, ACS has diminished by 19.15% resulting from a 40% increment of wind speed. In general, increasing solar radiation leads to decreasing and increasing the optimal number of wind turbines and solar panels, respectively. Based

Table 8
The mass of CO_2 gas produced by diesel engine generators at different LPSP and REP standards.

CO_2 (ton per year)								
Hybrid system	$LPSP_{max}$ (%)							
	0	1	3	5	10	1	1	1
	REP_{min} (%)							
	95	95	95	95	95	91	93	97
PV/WTG/BESS/DEG	10.688	5.638	5.465	3.615	3.739	10.320	8.890	3.450
PV/BESS/DEG	11.791	6.926	4.528	4.751	3.228	12.220	11.319	3.950
WTG/BESS/DEG	12.829	5.645	5.513	5.336	3.532	13.538	9.415	3.950
DEG	$LPSP_{max}$ (%)							
	0	1	3	5	10			
	90.067	89.268	87.575	85.937	83.500			

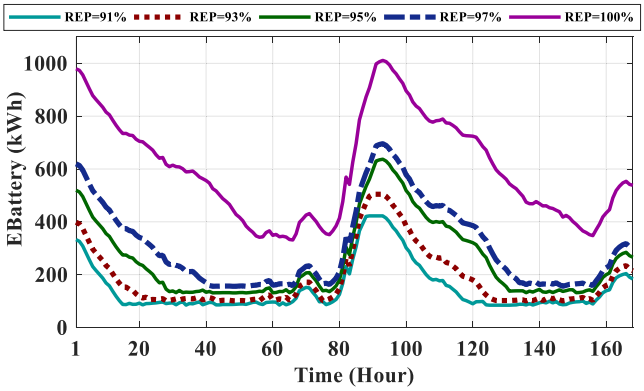

Fig. 30. Amount of stored energy in BESSs from 1st to 7th January for WTG/BESS/DEG strategy at $LPSP_{max} = 1\%$.

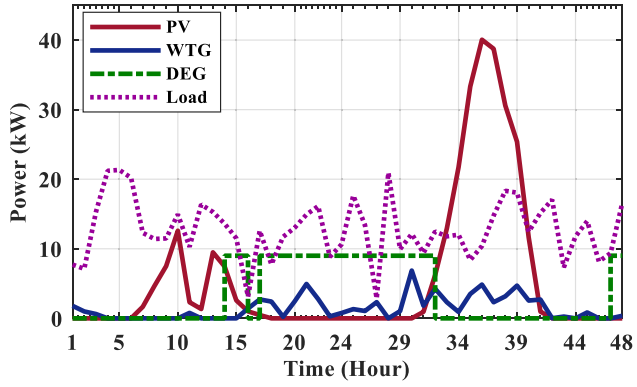

Fig. 31. The pattern of power generated by PV/WTG/BESS/DEG strategy from 1st to 2nd January at $LPSP_{max} = 3\%$, $REP_{min} = 95\%$.

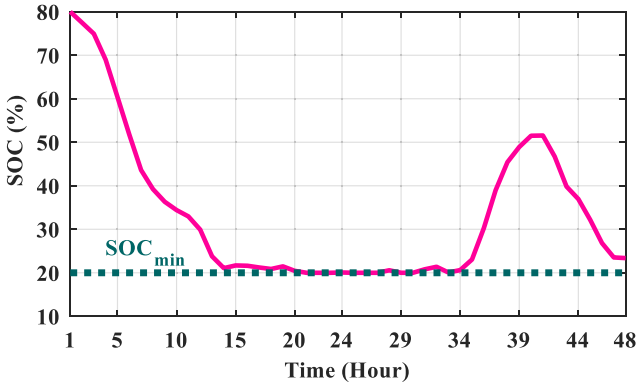

Fig. 32. The behavior of discharge state of battery bank during 1th to 2nd January at $LPSP_{max} = 3\%$, $REP_{min} = 95\%$.

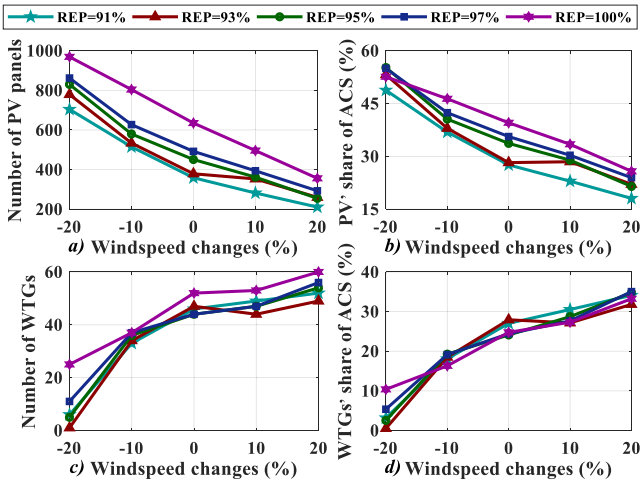

Fig. 33. Sensitivity analysis of wind speed on number of PV panels (a), the share of PV panels in the ACS (b), number of wind turbine generators (c), and the share of wind turbine generators in the ACS (d) for PV/WTG/BESS/DEG strategy at $LPSP_{max} = 1\%$.

on Fig. 34, with a 40% increase in radiation (from −20% to + 20% real radiation) at $REP_{min} = 91\%$, the number of PV panels has increased from 331 to 381 and the optimal number of wind turbine generators has decreased from 58 to 33. In this case, the total annual cost of the system has decreased by 10.61%, which is 8.53% less than the case of a 40% increase in wind speed.

5.7.2. Price of fuel

The impact of different behaviors of fuel price on the optimal *ACS* (\$), *REP* (%), the fuel consumption of diesel engine generators (Liter per year), and the annual mass of CO_2 produced by DEGs (ton), are depicted in Fig. 35a, 35b, 35c, and 35d for PV/WTG/BESS/DEG configuration for different REP_{min} and $LPSP_{max}$. According to Fig. 35, the annualized cost of the hybrid system and renewable energy penetration can be affected by increment of the cost of fossil fuel. In contrast, the consumption of fuel as well as the amount of emitted CO_2 witnesses a downward trend. This means that growth of fuel cost could lead to increasing production of renewable energy resources as well as decline in using diesel engine generators. As a proper example, for $LPSP_{max} = 10\%$, $REP_{min} = 91\%$, and 50% rise in the expenditure on fuel, the number of DEG drops to zero value. Moreover, the optimal number of PV and BESS increase from 311 and 172 to 411 and 228, respectively. In this case, the renewable energy penetration experiences a growth to 100% and as a result, the amount of greenhouse gas emission will reach zero level, as well.

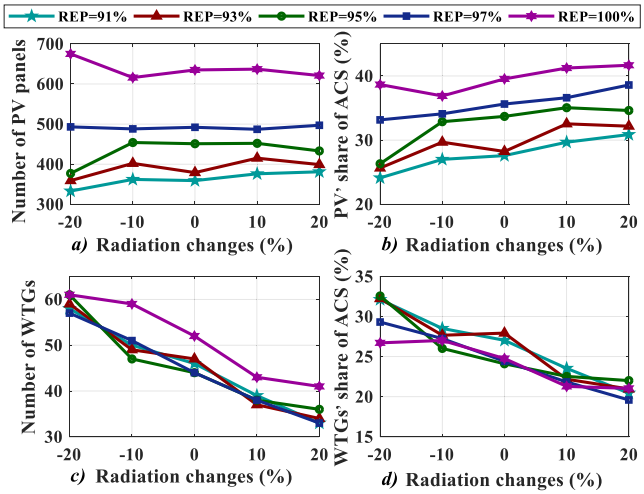

Fig. 34. Sensitivity analysis of radiation on number of PV panels (a), the share of PV panels in the ACS (b), number of wind turbine generators (c), and the share of wind turbine generators in the ACS (d) for PV/WTG/BESS/DEG strategy at $LPSP_{\max} = 1\%$.

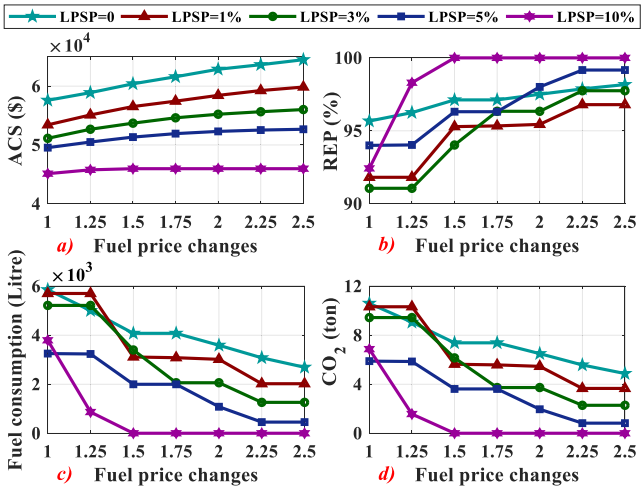

Fig. 35. Sensitivity analysis of fuel price on the annualized cost of the system (a), renewable energy penetration (b), the fuel consumption of diesel engine generators (c), the mass of CO_2 produced by diesel engine generators (d) for PV/WTG/BESS/DEG strategy at $REP_{\min} = 91\%$.

5.7.3. Lifespan of battery

To evaluate the effect of changes in the different lifespan of battery energy storage systems on the number of batteries, the annualized cost of the system (%), and the excess production of power (kW), Fig. 36(a–c) are presented. It is obvious that the optimal number of batteries experiences a growth by increment of the lifespan of BESS. On the contrary, two other items including ACS and excess power decline at different values of REP_{min}.

6. Conclusion

In inaccessible areas, based on the geographical location, different contributions of renewable energy sources can be introduced considering several constraints related to supportive sources of energy like diesel engine generators. From this perspective, an optimal sizing of a real hybrid system was investigated in light of a real case study in the Sistan & Balouchestan province of Iran in this paper. Since accurate weather data was not readily available for use in control centers, an adaptive neuro-fuzzy based on fuzzy c-means (ANFIS-FCM) clustering technique was proposed to anticipate wind speed, ambient temperature, and solar radiation data. multi-verse optimizer (MVO) demonstrated a more satisfactory performance considering renewable energy penetration (REP) and loss of power supply probability (LPSP) indexes compared to another mentioned optimization approaches e.g., GOA, GWO, DA, and SSA. Simulation results depicted that PV/WTG/BESS/DEG contribution was considered as the most cost-effective strategy in terms of the annualized cost of the system for different levels of reliability (from 0% to 10%) and renewable energy penetration level (from 90% to 100%) compared to other scenarios. Based on obtained experiences, this pattern could be implemented to improve the reliability of load demand in remote areas. Furthermore, deployment of meta-heuristic algorithms, along with intelligent weather forecasting is suggested to resolve complex energy management planning in distant sites efficiently. Finally, CO_2 emission and the effect of change in wind speed, solar radiation, the lifespan of battery energy storage systems, and the fuel price of diesel engine generators on annualize cost of system were reported at different values of $LPSP_{max}$ and REP_{min}.

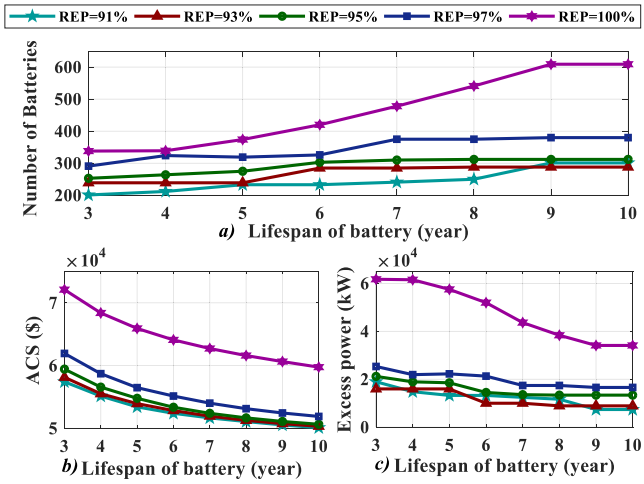

Fig. 36. Sensitivity analysis of battery lifespan on number of batteries (a), the annualized cost of the hybrid system (b), excess power generated by the hybrid system (c) for PV/WTG/BESS/DEG strategy at $LPSP_{\max} = 1\%$.

CRediT authorship contribution statement

Ahmadreza Abazari: Conceptualization, Methodology, Software, Formal analysis, Resources, Data curation, Writing – original draft. **Mohammad Mahdi Soleymani:** Conceptualization, Methodology, Software, Formal analysis. **Innocent Kamwa:** Validation, Writing - review & editing, Supervision, Project administration. **Masoud Babaei:** Validation, Resources, Data curation. **Mohsen Ghafouri:** Validation, Investigation, Writing – original draft, Writing – review & editing. **S.M. Muyeen:** Validation, Investigation, Writing – review & editing, Supervision, Project administration. **Aoife M. Foley:** Supervision, Project administration.

Declaration of competing interest

The authors declare that they have no known competing financial interests or personal relationships that could have appeared to influence the work reported in this paper.

Acknowledgment

All authors have read and agreed to the published version of the manuscript.

References

Abazari, A., Soleymani, M.M., Babaei, M., Ghafouri, M., Monsef, H., Beheshti, M.T.H., 2020. High penetrated renewable energy sources-based AOMPC for microgrid's frequency regulation during weather changes, time-varying parameters and generation unit collapse. IET Gener. Transm. Distrib. 14, 5164–5182.

Abdulshahed, A.M., Longstaff, A.P., Fletcher, S., 2015a. The application of ANFIS prediction models for thermal error compensation on CNC machine tools. Appl. Soft Comput. 27, 158–168.

Abdulshahed, A.M., Longstaff, A.P., Fletcher, S., 2015b. The application of ANFIS prediction models for thermal error compensation on CNC machine tools. Appl. Soft Comput. 27, 158–168.

Alberizzi, J.C., Frigola, J.M., Rossi, M., Renzi, M., 2020. Optimal sizing of a Hybrid Renewable Energy System: Importance of data selection with highly variable renewable energy sources. Energy Convers. Manage. 223, 113303.

Ali, E.E., El-Hameed, M.A., El-Fergany, A.A., El-Arini, M.M., 2016. Parameter extraction of photovoltaic generating units using multi-verse optimizer. Sustain. Energy Technol. Assess. 17, 68–76.

Alturki, F.A., Al-Shamma'a, A.A., Farh, H.M.H., AlSharabi, K., 2021. Optimal sizing of autonomous hybrid energy system using supply–demand-based optimization algorithm. Int. J. Energy Res. 45, 605–625.

Arzani, M., Abazari, A., Oshnoei, A., Ghafouri, M., Muyeen, S.M., 2021. Optimal distribution coefficients of energy resources in frequency stability of hybrid microgrids connected to the power system. Electronics 13, 1591.

Ashraf, M.A., Liu, Z., Alizadeh, A.a., Nojavan, S., Jermsittiparsert, K., Zhang, D., 2020. Designing an optimized configuration for a hybrid PV/Diesel/Battery energy system based on metaheuristics: A case study on Gobi Desert. J. Cleaner Prod. 270, 122467.

Askarzadeh, A., 2017. Electrical power generation by an optimised autonomous PV/wind/tidal/battery system. IET Renew. Power Gener. 11, 152–164.

Askarzadeh, A., dos Santos Coelho, L., 2015. A novel framework for optimization of a grid independent hybrid renewable energy system: A case study of Iran. Sol. Energy 112, 383–396.

Babaei, M., Abazari, A., Soleymani, M.M., Ghafouri, M., Muyeen, S.M., Beheshti, M.T.H., 2021. A data-mining based optimal demand response program for smart home with energy storages and electric vehicles. J. Energy Storage 36.

Bala, B.K., Siddique, S.A., 2009. Optimal design of a PV-diesel hybrid system for electrification of an isolated island—Sandwip in Bangladesh using genetic algorithm. Energy Sustain. Dev. 13, 137–142.

Bayani, R., Bushlaibi, M., Manshadi, S.D., 2021a. Short-term operational planning problem of the multiple-energy carrier hybrid ac/dc microgrids. In: 2021 IEEE PES General Meeting.

Bayani, R., Manshadi, S.D., Liu, G., Wang, Y., Dai, R., 2021b. Autonomous charging of electric vehicle fleets to enhance renewable generation dispatchability. in CSEE J. Power Energy Syst..

Das, B.K., Zaman, F., 2019. Performance analysis of a PV/Diesel hybrid system for a remote area in Bangladesh: Effects of dispatch strategies, batteries, and generator selection. Energy 169, 263–276.

Foley, A.M., Gallachóir, B.P.Ó., Hur, J., Baldick, R., McKeogh, E.J., 2010. A strategic review of electricity systems models. Energy 35, 4522–4530.

Ghaffari, A., Askarzadeh, A., 2020. Design optimization of a hybrid system subject to reliability level and renewable energy penetration. Energy 193, 116754.

Ghorbani, N., Kasaeian, A., Toopshekan, A., Bahrami, L., Maghami, A., 2018. Optimizing a hybrid wind-PV-battery system using GA-PSO and MOPSO for reducing cost and increasing reliability. Energy 154, 581–591.

Hafez, O., Bhattacharya, K., 2012. Optimal planning and design of a renewable energy based supply system for microgrids. Renew. Energy 45, 7–15.

Haratian, M., Tabibi, P., Sadeghi, M., Vaseghi, B., Poustdouz, A., 2018. A renewable energy solution for stand-alone power generation: A case study of Khshu Site-Iran. Renew. Energy 125, 926–935.

Hossain, M.A., Pota, H.R., Squartini, S., Abdou, A.F., 2019. Modified PSO algorithm for real-time energy management in grid-connected microgrids. Renew. Energy 136, 746–757.

Jamshidi, M., Askarzadeh, A., 2019. Techno-economic analysis and size optimization of an off-grid hybrid photovoltaic, fuel cell and diesel generator system. Sustainable Cities Soc. 44, 310–320.

Kazem, H.A., Khatib, T., Sopian, K., 2013. Sizing of a standalone photovoltaic/battery system at minimum cost for remote housing electrification in sohar, oman. Energy Build. 61, 108–115.

Khan, A., Alghamdi, T.A., Khan, Z.A., Fatima, A., Abid, S., Khalid, A., Javaid, N., 2019. Enhanced evolutionary sizing algorithms for optimal sizing of a stand-Alone PV-WT-battery hybrid system. Appl. Sci. 9, 5197.

Lee, DJ., Wang, L., 2008. Small-signal stability analysis of an autonomous hybrid renewable energy power generation/energy storage system part I: Time-domain simulations. IEEE Trans Energy Convers. 23 (1), 311–320.

Maleki, A., Askarzadeh, A., 2014a. Artificial bee swarm optimization for optimum sizing of a stand-alone PV/WT/FC hybrid system considering LPSP concept. Sol. Energy 107, 227–235.

Maleki, A., Askarzadeh, A., 2014b. Optimal sizing of a PV/wind/diesel system with battery storage for electrification to an off-grid remote region: A case study of Rafsanjan, Iran. Sustain. Energy Technol. Assess. 7, 147–153.

Maleki, A., Pourfayaz, F., 2015. Optimal sizing of autonomous hybrid photovoltaic/wind/battery power system with LPSP technology by using evolutionary algorithms. Sol. Energy 115, 471–483.

Mirjalili, S., 2016. Dragonfly algorithm: a new meta-heuristic optimization technique for solving single-objective, discrete, and multi-objective problems. Neural Comput. Appl. 27, 1053–1073.

Mirjalili, S., Gandomi, A.H., Mirjalili, S.Z., Saremi, S., Faris, H., Mirjalili, S.M., 2017. Salp Swarm Algorithm: A bio-inspired optimizer for engineering design problems. Adv. Eng. Softw. 114, 163–191.

Mirjalili, S., Mirjalili, S.M., Hatamlou, A., 2016. Multi-Verse Optimizer: a nature-inspired algorithm for global optimization. Neural Comput. Appl. 27, 495–513.

Mirjalili, S., Mirjalili, S.M., Lewis, A., 2014. Grey wolf optimizer. Adv. Eng. Softw. 69, 46–61.

Mirrashid, M., 2014. Earthquake magnitude prediction by adaptive neuro-fuzzy inference system (ANFIS) based on fuzzy C-means algorithm. Nat. Hazards 74, 1577–1593.

Mohammadi, Z., Limaei, S.M., Shahraji, T.R., 2017. Linear programming approach for optimal forest plantation. J. For. Res. 28, 299–307.

Movahediyan, Z., Askarzadeh, A., 2018. Multi-objective optimization framework of a photovoltaic-diesel generator hybrid energy system considering operating reserve. Sustainable Cities Soc. 41, 1–12.

Ranjbar, M.R., Kouhi, S., 2015. Sources' response for supplying energy of a residential load in the form of on-grid hybrid systems. Int. J. Electr. Power Energy Syst. 64, 635–645.

Ranjbar, M.R., Mohammadian, M., esmaili, S., 2014. Economic analysis of hybrid system consists of fuel cell and wind based CHP system for supplying grid-parallel residential load. Energy Build. 68, 476–487.

Razmjoo, A., Shirmohammadi, R., Davarpanah, A., Pourfayaz, F., Aslani, A., 2019. Stand-alone hybrid energy systems for remote area power generation. Energy Rep. 5, 231–241.

Roy, S., 1997. Optimal planning of wind energy conversion systems over an energy scenario. IEEE Trans. Energy Convers. 12, 248–254.

Sabahi, K., Teshnehlab, M., shoorhedeli, M.A., 2009. Recurrent fuzzy neural network by using feedback error learning approaches for LFC in interconnected power system. Energy Convers. Manage. 50, 938–946.

Salameh, T., Ghenai, C., Merabet, A., Alkasrawi, M., 2020. Techno-economical optimization of an integrated stand-alone hybrid solar PV tracking and diesel generator power system in Khorfakkan, United Arab Emirates. Energy 190, 116475.

Sanajaoba, S., Fernandez, E., 2016. Maiden application of Cuckoo search algorithm for optimal sizing of a remote hybrid renewable energy system. Renew. Energy 96, 1–10.

Sanajaoba Singh, S., Fernandez, E., 2018. Modeling, size optimization and sensitivity analysis of a remote hybrid renewable energy system. Energy 143, 719–731.

Saremi, S., Mirjalili, S., Lewis, A., 2017. Grasshopper optimisation algorithm: Theory and application. Adv. Eng. Softw. 105, 30–47.

Shukri, arah E., Al-Sayyed, Rizik, Hudaib, Amjad, Mirjalili, Seyedali, 2021. Enhanced multi-verse optimizer for task scheduling in cloud computing environments. Expert Syst. Appl. 168, 114230.

Stoppato, A., Cavazzini, G., Ardizzon, G., Rossetti, A., 2014. A PSO (particle swarm optimization)-based model for the optimal management of a small PV(Photovoltaic)-pump hydro energy storage in a rural dry area. Energy 76, 168–174.

Suresh, V., Muralidhar, M., Kiranmayi, R., 2020. Modelling and optimization of an off-grid hybrid renewable energy system for electrification in a rural areas. Energy Rep. 6, 594–604.

Zhang, W., Maleki, A., Rosen, M.A., Liu, J., 2018. Optimization with a simulated annealing algorithm of a hybrid system for renewable energy including battery and hydrogen storage. Energy 163, 191–207.

Zhang, W., Maleki, A., Rosen, M.A., Liu, J., 2019. Sizing a stand-alone solar-wind-hydrogen energy system using weather forecasting and a hybrid search optimization algorithm. Energy Convers. Manage. 180, 609–621.